



Gdański Uniwersytet Medyczny

Wydział Lekarski

Rozprawa doktorska

**Ocena tkanki tłuszczowej i mięśniowej
metodą rezonansu magnetycznego w populacji pediatrycznej**

Assessment of adipose and muscle tissue with magnetic resonance imaging
in pediatric population

lek. Kacper Marunowski

I Zakład Radiologii
Gdańskiego Uniwersytetu Medycznego

Promotor: dr hab. n. med. Maciej Piskunowicz
I Zakład Radiologii
Gdańskiego Uniwersytetu Medycznego

Promotor pomocniczy: dr n. med. Dominik Świętoń
II Zakład Radiologii
Gdańskiego Uniwersytetu Medycznego

Gdańsk 2022

Składam serdeczne podziękowania

Mojemu promotorowi dr hab. n. med. Maciejowi Piskunowiczowi oraz promotorowi pomocniczemu dr n. med. Dominikowi Świętoniowi za umożliwienie rozwoju naukowego.

Współautorom artykułów wchodzących w skład rozprawy doktorskiej za owocną współpracę.

Moim Bliskim za okazane wsparcie.

SPIS TREŚCI

WYKAZ PRAC WCHODZĄCYCH W SKŁAD ROZPRAWY DOKTORSKIEJ / LIST OF MANUSCRIPTS INCLUDED IN THE DOCTORAL DISSERTATION.....	4
SŁOWA KLUCZOWE / KEY WORDS.....	5
STRESZCZENIE W JĘZYKU POLSKIM	6
I. WYKAZ STOSOWANYCH SKRÓTÓW.....	6
II. WPROWADZENIE.....	7
III. CELE PRACY	8
IV. OMÓWIENIE PUBLIKACJI WCHODZĄCYCH W SKŁAD ROZPRAWY DOKTORSKIEJ.....	9
i. Publikacja 1.....	9
ii. Publikacja 2.....	10
V. PODSUMOWANIE.....	12
SUMMARY IN ENGLISH.....	13
I. LIST OF ABBREVIATIONS.....	13
II. INTRODUCTION	14
III. AIMS OF THE STUDY.....	15
IV. DESCRIPTION OF THE PUBLICATIONS INCLUDED IN THE DOCTORAL THESIS	16
i. Publication 1.....	16
ii. Publication 2.....	17
V. SUMMARY	18
BIBLIOGRAFIA / REFERENCES	19
PUBLIKACJE WCHODZĄCE W SKŁAD ROZPRAWY DOKTORSKIEJ / MANUSCRIPTS INCLUDED IN THE DOCTORAL DISSERTATION	22

WYKAZ PRAC WCHODZĄCYCH W SKŁAD ROZPRAWY DOKTORSKIEJ / LIST OF
MANUSCRIPTS INCLUDED IN THE DOCTORAL DISSERTATION

Marunowski K, Świętoń D, Bzyl W, Grzywińska M, Kaszubowski M, Bandosz P, Khirichenko D,
Piskunowicz M

**MRI-derived subcutaneous and visceral adipose tissue reference values for children aged 6
to under 18 years.**

Front Nutr. 2021;8:757274. doi:10.3389/fnut.2021.757274

IF 6.590 | MNiSW: 70 pkt | praca oryginalna

Marunowski K, Świętoń D, Bzyl W, Grzywińska M, Bandosz P, Khirichenko D, Piskunowicz M

**Reference values for MRI-derived psoas and paraspinal muscles and macroscopic fat
infiltrations in paraspinal muscles in children.**

J Cachexia Sarcopenia Muscle. 2022;10.1002/jcsm.13049. doi:10.1002/jcsm.13049

IF: 12.063 | MNiSW: 200 pkt | praca oryginalna

SŁOWA KLUCZOWE / KEY WORDS

Tkanka tłuszczowa podskórna, tkanka tłuszczowa wisceralna, tłuszcz wewnątrzmięśniowy, mięśnie lędźwiowe i przykręgosłupowe, wartości referencyjne, siatki centylowe, dzieci, obrazowanie rezonansu magnetycznego, sarkopenia, ocena stanu odżywienia

Subcutaneous adipose tissue, visceral adipose tissue, intramuscular fat, psoas and paraspinal muscles, reference values, percentile charts, children, magnetic resonance imaging, sarcopenia, nutritional assessment

STRESZCZENIE W JĘZYKU POLSKIM

I. WYKAZ STOSOWANYCH SKRÓTÓW

BIA	(<i>ang. bioelectrical impedance analysis</i>), analiza impedancji bioelektrycznej
BMI	(<i>ang. body mass index</i>), wskaźnik masy ciała
CT	(<i>ang. computed tomography</i>), tomografia komputerowa
L	(<i>ang. lumbar</i>), lędźwiowy
MR	(<i>ang. magnetic resonance</i>), rezonans magnetyczny
MSD	MedStream Designer
pMRI	parametric MRI
PSMA	(<i>ang. paraspinal muscle area</i>), powierzchnia mięśni przykręgosłupowych
SAT	(<i>ang. subcutaneous adipose tissue</i>), tkanka tłuszczowa podskórna
tMFI	(<i>ang. total macroscopic fat infiltrations</i>), całkowita powierzchnia makroskopowych infiltracji tkanki tłuszczowej w obrębie mięśni przykręgosłupowych
tPMA	(<i>ang. total psoas muscle area</i>), całkowita powierzchnia mięśni lędźwiowych większych
tPSMA	(<i>ang. total paraspinal muscle area</i>), całkowita powierzchnia mięśni przykręgosłupowych
VAT	(<i>ang. visceral adipose tissue</i>), tkanka tłuszczowa wisceralna
WtHR	(<i>ang. waist to height ratio</i>), stosunek obwodu talii do wysokości ciała

II. WPROWADZENIE

Nadwaga i otyłość w populacji pediatrycznej są definiowane jako wartość BMI odpowiednio powyżej 85-go i 95-go percentyla względem norm właściwych dla wieku i płci zawartych w siatkach centylowych.¹ Stanowią one niezależny czynnik ryzyka rozwoju chorób sercowo-naczyniowych, cukrzycy, depresji oraz chorób nowotworowych w wieku dorosłym.^{2,3} Sarkopenia u dzieci jest nowym pojęciem powiązaniem z niedostateczną ilością tkanki mięśniowej względem wieku. Udowodniono, że sarkopenia wpływa na częstość występowania powikłań pooperacyjnych oraz komplikacji związanych z leczeniem przeciwnowotworowym.⁴⁻⁷ W związku z powyższym wczesne wykrycie zaburzeń składu ciała jest niezbędne dla zapewnienia prawidłowego rozwoju dzieci, szczególnie w przypadku współistnienia chorób przewlekłych i nowotworowych.^{8,9} Obecnie analiza składu ciała oraz dystrybucji tkanki tłuszczowej staje się istotnym elementem oceny stanu pacjenta w ramach opieki specjalistycznej. Podstawowymi narzędziami wykorzystywanymi w praktyce klinicznej są pomiary antropometryczne służące m.in. do określenia parametrów takich jak BMI czy WtHR. Metody te charakteryzują się jednak dużym błędem pomiaru i zaniżają rzeczywistą częstość występowania otyłości u dzieci.¹⁰⁻¹² W dużych ośrodkach klinicznych skład ciała coraz częściej oceniany jest na podstawie pomiaru impedancji tkanek. BIA opiera się na założeniu stałości składu chemicznego beztłuszczowej masy ciała i w populacji osób zdrowych pozwala na uzyskanie dokładniejszych wyników niż przy użyciu pomiarów antropometrycznych.^{13,14} Jednakże interwencje chirurgiczne oraz stany patologiczne, takie jak wodobrzusze czy organomegalia, wpływają negatywnie na precyzję pomiarów.¹⁵ Użyteczność badań CT oraz MR w ocenie tkanki mięśniowej i tłuszczowej została udowodniona zarówno u dzieci, jak i u osób dorosłych.¹⁶⁻¹⁹ Obie metody pozwalają nie tylko na bezpośrednią, ilościową ocenę tkanek, ale również na wydzielenie ich kompartmentów takich jak SAT i VAT w obrębie tkanki tłuszczowej. W związku z narażeniem na promieniowanie jonizujące badania CT u dzieci są wykonywane głównie w stanach zagrożenia życia, podczas gdy obrazowanie MR stanowi nieodłączoną część procesu diagnostycznego oraz badań kontrolnych w przebiegu wielu chorób u dzieci. Jest to metoda bezpieczna, która ze względu na wysoką rozdzielczość tkankową stanowi złoty standard wśród metod oceny składu ciała.¹⁹⁻²¹ Niemniej jednak ilościowa ocena tkanki tłuszczowej i mięśniowej w oparciu o badanie MR całego ciała nie została do tej pory wdrożona do

praktyki klinicznej. Związane jest to z wysokim kosztem badania, długim czasem akwizycji obrazów oraz potrzebą zaangażowania wysoko wyspecjalizowanego personelu medycznego do prawidłowej analizy obrazów przy użyciu narzędzi do ręcznej i półautomatycznej segmentacji tkanek. W świetle ostatnich doniesień ocena pojedynczych przekrojów na poziomie jamy brzusznej dobrze koreluje z całkowitą masą mięśniową oraz ilością SAT i VAT.²¹⁻²⁴ Rozszerzenie oceny badań MR o segmentację tkanek na pojedynczych przekrojach może pozwolić na wcześniejsze wykrycie zaburzeń składu ciała i umożliwić adekwatne leczenie żywieniowe.

III. CELE PRACY

1. Stworzenie zależnych od płci i wieku wartości referencyjnych podskórnej oraz wisceralnej tkanki tłuszczowej w obrazach rezonansu magnetycznego w populacji pediatrycznej.
2. Stworzenie zależnych od płci i wieku wartości referencyjnych mięśni lędźwiowych oraz przykręgosłupowych w obrazach rezonansu magnetycznego w populacji pediatrycznej.
3. Wyznaczenie wartości referencyjnych infiltracji tkanki tłuszczowej w obrębie mięśni przykręgosłupowych w populacji pediatrycznej.

IV. OMÓWIENIE PUBLIKACJI WCHODZĄCYCH W SKŁAD ROZPRAWY DOKTORSKIEJ

i. Publikacja 1.

MRI-Derived Subcutaneous and Visceral Adipose Tissue Reference Values for Children Aged 6 to Under 18 Years.

Celem pierwszej publikacji było opracowanie wartości referencyjnych SAT i VAT w populacji pediatrycznej. Do pracy włączono 262 badania MR jamy brzusznej i miednicy mniejszej zdrowych dzieci w wieku od 6 do 18 lat (111 dziewczynek i 151 chłopców). Badania wykonane w latach 2010-2020 zostały wyszukane z lokalnej bazy danych przy pomocy oprogramowania MSD. Z ostatecznej analizy wykluczono badania dzieci w wieku od 0 do 5 lat ze względu na zbyt małą liczebność grupy. Półautomatyczna segmentacja tkanki tłuszczowej została przeprowadzona przez dwóch obserwatorów w programie pMRI. Wyodrębniono tkankę tłuszczową umiejscowioną na zewnątrz od mięśni jamy brzusznej i grzbietu (SAT) oraz tkankę tłuszczową wewnątrz jamy brzusznej z wyłączeniem infiltracji wewnątrzmięśniowych (VAT). Segmentacja tkanki tłuszczowej w populacji osób dorosłych najczęściej przeprowadzana jest w oparciu o T1-zależne sekwencje Dixon. Cechują się one dużą podatnością na artefakty ruchowe, w związku z tym jakość badania jest silnie zależna od umiejętności wstrzymania oddechu podczas akwizycji obrazu. Niestety współpraca dzieci w czasie badania jest często ograniczona, a w przypadku zastosowania sedacji w najmłodszej grupie wiekowej niemożliwa. W związku z mniejszą ilością artefaktów ruchowych oraz porównywalną czułością i swoistością segmentacji tkanki tłuszczowej w obrazach T1- oraz T2-zależnych, do analizy wykorzystano obrazy T2-zależne. Ocenie poddany został przekrój poprzeczny na poziomie trzonu kręgu L2, który najlepiej odzwierciedla całkowitą ilość SAT i VAT u dzieci. Obaj obserwatorzy przeprowadzili segmentację badań 15 pacjentów. Na podstawie uzyskanych wyników oceniono powtarzalność pomiarów przy pomocy wykresów Blanda-Altmana. Różnice pomiędzy pomiarami tego samego obserwatora, jak również między dwoma obserwatorami wynosiły do 1% dla SAT (średnia różnica 0.07 cm²) oraz do 3% dla VAT (średnia różnica 0.04-0.08 cm²). Wysoka powtarzalność oznaczeń pozwoliła na wykorzystanie pomiarów SAT i VAT do stworzenia wartości referencyjnych. Siatki centylowe SAT, VAT i BMI zależne od płci i wieku zostały opracowane w oparciu o metodę lambda-mu-

sigma przy użyciu programu LMSChartMaker. Analiza uzyskanych wartości referencyjnych wykazała podobny rozkład linii centylowych BMI w porównaniu z dostępnymi normami WHO. Dystrybucja linii centylowych SAT różniła się pomiędzy płciami. U chłopców obserwowano wzrost wartości we wszystkich grupach wiekowych (mediana 66.33 cm² w 18. roku życia), natomiast u dziewczynek wartości ustabilizowały się około 14. roku życia (mediana 91.1 cm²). U obu płci wykazano ciągły wzrost pola powierzchni VAT w całym obserwowanym okresie, z osiągnięciem mediany 55.08 cm² u chłopców i 48.41 cm² u dziewczynek w 18. roku życia. Obserwowano różnicę dystrybucji tkanki tłuszczowej pomiędzy płciami z przewagą SAT u dziewczynek oraz VAT u chłopców. Wartości 85. i 95. percentyla na siatkach centylowych BMI uznawane są za punkty ocięcia dla nadwagi i otyłości. W związku z narastającym problemem nadmiernej masy ciała w populacji pediatrycznej wyznaczono korespondujące linie centylowe dla SAT i VAT.

ii. Publikacja 2.

Reference values for MRI-derived psoas and paraspinal muscles and macroscopic fat infiltrations in paraspinal muscles in children.

Celem drugiej publikacji było opracowanie wartości referencyjnych dla tPMA, tPSMA oraz tMFI w populacji pediatrycznej. Do pracy włączono 465 badań MR jamy brzusznej, miednicy mniejszej oraz kręgosłupa w odcinku lędźwiowym zdrowych dzieci w wieku od 1 do 18 lat (233 dziewczynki i 232 chłopców). Badania wykonane w latach 2010-2021 zostały wyszukane z lokalnej bazy danych przy pomocy MSD. Z ostatecznej analizy wykluczono badania dzieci w pierwszym roku życia ze względu na zbyt małą liczebność grupy. Półautomatyczna segmentacja tkanek została przeprowadzona przez dwóch obserwatorów w programie pMRI. Wyodrębniono PSMA definiowane jako sumę powierzchni mięśni wielodzielnego, biodrowo-żebrowego lędźwi oraz najdłuższego lędźwi. Sumę powierzchni mięśni po obu stronach ciała oznaczono jako tPMA, tPSMA i tMFI. Pole powierzchni tMFI zostało wyłączone z analizy obszaru tPSMA. Segmentację tkanek przeprowadzono w oparciu o standardowe obrazy T2-zależne na poziomie krążka międzykręgowego L4, który dobrze koreluje z całkowitą masą mięśniową. W przypadku objęcia krążka międzykręgowego L4 na więcej niż jednym przekroju do analizy wykorzystano obrazy zlokalizowane bliżej trzonu

kręgu L4. Powtarzalność pomiarów została oceniona przy pomocy wykresów Blanda-Altmana w oparciu o 40 badań segmentowanych przez obu obserwatorów. Różnice pomiędzy pomiarami tego samego obserwatora, jak również między dwoma obserwatorami wynosiły średnio 0.39-0.43 cm² dla tPMA oraz 0.05-0.1 cm² dla tPSMA. Wysoka powtarzalność segmentacji pozwoliła na wykorzystanie pomiarów tPMA, tPSMA i tMFA do stworzenia zależnych od płci i wieku siatek centylowych. Wartości referencyjne BMI, wagi, tkanki mięśniowej i tłuszczowej zostały opracowane w oparciu o metodę lambda-mu-sigma przy użyciu programu LMSChartMaker. Uzyskane siatki centylowe BMI porównano z narodowymi wartościami referencyjnymi (badanie Ola/Olaf).^{25,26} Włączona do badania populacja charakteryzowała się wyższym BMI, szczególnie dla zakresu +2SD i +1SD (do 2,7 jednostki u dziewczynek oraz 1,46 jednostki u chłopców). W pierwszych latach życia przebieg linii centylowych grup mięśniowych u obu płci był podobny, z następczą predominacją u chłopców od odpowiednio 8. i 10. roku życia dla tPMA i tPSMA. U dziewczynek zwracało uwagę wypłaszczenie linii centylowych od około 14. roku życia z osiągnięciem median równych 26.37cm² dla tPMA i 40.76cm² dla tPSMA na końcu obserwowanego zakresu. Taki przebieg krzywych może być związany z wcześniejszym zakończeniem okresu wzrastania w populacji żeńskiej. U chłopców dynamiczny wzrost pól powierzchni tPMA i tPSMA widoczny był we wszystkich grupach wiekowych, z osiągnięciem median równych 40.43cm² i 56.66cm² w 18. roku życia. W porównaniu z wynikami kanadyjskiego badania opartego na obrazowaniu CT, wartości 75., 90., i 95. percentyli wykazały nieco większą wariację, jednak ogólny przebieg linii centylowych był podobny.²¹ W wieku od 1 do 3 lat pole powierzchni tMFI było porównywalne u obu płci, w pozostałym obserwowanym zakresie większą ilość tkanki tłuszczowej obserwowano u dziewczynek. Średnia ilość tMFI była zbieżna z wcześniejszymi badaniami i wyniosła około 5% (SD ±3.65%) u dziewczynek i około 3.5% (SD ±2.25%) u chłopców.

V. PODSUMOWANIE

Wyniki przeprowadzonych badań umożliwiły stworzenie po raz pierwszy wartości referencyjnych SAT, VAT, tPMA, tPSMA i tMFI opartych na badaniach MR w populacji pediatrycznej. Ilościowa ocena tkanki tłuszczowej oraz tkanki mięśniowej w badaniu MR może pozwolić na wcześniejsze wykrycie zaburzeń składu ciała i personalizację planu leczenia. Szerokie wykorzystanie badań MR w standardowych protokołach diagnostycznych u dzieci otwiera możliwość wykorzystania zaproponowanej metody w praktyce klinicznej.

SUMMARY IN ENGLISH

I. LIST OF ABBREVIATIONS

BIA	bioelectrical impedance analysis
BMI	body mass index
CT	computed tomography
L	lumbar
MR	magnetic resonance
MSD	MedStream Designer
pMRI	parametric MRI
PSMA	paraspinal muscle area
SAT	subcutaneous adipose tissue
tMFI	total macroscopic fat infiltrations
tPMA	total psoas muscle area
tPSMA	total paraspinal muscle area
VAT	visceral adipose tissue
WtHR	waist to height ratio

II. INTRODUCTION

Overweight and obesity in the pediatric population are defined as BMI values at the level of 85th and 95th percentiles based on age and sex dependent percentile charts.¹ Childhood overweight and obesity have been recognized as an independent risk factor for the development of cardiovascular diseases, diabetes, depression and neoplastic diseases in adulthood.²⁻³ Pediatric sarcopenia is a new term associated with insufficient muscle mass at a given age and it affects prevalence of surgical and anticancer treatment complications.⁴⁻⁷ Therefore, early detection of body composition disorders is essential to ensure the proper development of children, especially in the presence of chronic and neoplastic diseases.⁸⁻⁹ Currently, body composition analysis and assessment of adipose tissue distribution are becoming an important part of the patients' evaluation during hospitalization. In clinical practice the routine approaches include anthropometric measurements to determine parameters such as BMI or WtHR. These methods are characterized by a large measurement error, and therefore they underestimate the actual prevalence of obesity in children.¹⁰⁻¹² In large clinical centers tissue impedance analysis has been increasingly used for body composition assessment. BIA is based on the assumption of constant chemical composition of fat-free-body and provides more precise results than anthropometric measurements in the healthy population.¹³⁻¹⁴ However, surgical interventions and pathological conditions such as ascites and organomegaly negatively affect its accuracy.¹⁵ The usefulness of CT and MR in the assessment of muscle and adipose tissue has already been proved in both adult and pediatric patients.¹⁶⁻¹⁹ Both methods allow for direct quantitative assessment of tissues and additionally enable segmentation of their compartments such as SAT and VAT within adipose tissue. In children due to radiation exposure the CT examinations are performed primarily during emergency, while diagnostic and control tests of multiple diseases are carried out using MR. MR is radiation-free technique, which due to its high tissue resolution is considered a gold standard among body composition assessment methods.¹⁹⁻²¹ Nevertheless, quantitative evaluation of adipose and muscle tissues based on whole body MR examination has not been introduced into clinical practice yet. This is related to long acquisition time of the images, associated costs and dependence on highly qualified personnel for proper image analysis based on manual and semi-automatic tissue segmentation tools. According to recent reports the assessment of single cross-sections at

the abdominal level correlates with total muscle mass and the amount of SAT and VAT.²¹⁻²⁴ Incorporation of single cross-section tissue segmentation into standard MR images analysis may enable earlier detection of body composition disorders and adequate nutritional treatment.

III. AIMS OF THE STUDY

1. Establishment of sex and age-dependent MR-derived reference normative values for SAT and VAT in pediatric population.
2. Establishment of sex and age-dependent MR-derived reference values for tPMA and tPSMA in pediatric population.
3. Establishment of reference values for tMFI in pediatric population.

IV. DESCRIPTION OF THE PUBLICATIONS INCLUDED IN THE DOCTORAL THESIS

i. Publication 1.

MRI-Derived Subcutaneous and Visceral Adipose Tissue Reference Values for Children Aged 6 to Under 18 Years.

The first publication aimed to develop SAT and VAT reference values in the pediatric population. The study included 262 MR examinations of abdomen and pelvis of healthy children aged from 6 to 18 years (111 girls and 151 boys). The local database was searched for examinations conducted in years 2010-2020 by means of MSD. The examinations of children aged 0-5 years were excluded from the final analysis due to the insufficient sample size. Semi-automatic adipose tissue segmentation was performed by two observers with the use of pMRI. The adipose tissue was separated into SAT, which is located outside of the abdominal and back muscles, and VAT defined as the adipose tissue inside the abdominal cavity excluding intramuscular infiltrations. In most studies segmentation of adipose tissue in the adult population was based on T1-weighted Dixon sequences. These sequences are vulnerable to movement artefacts, therefore the quality of acquired images is strongly dependent on the ability to breath-hold during the examination. Unfortunately, full cooperation is difficult in young children, and impossible in case of sedation in the youngest age group. Due to the lower number of movement artifacts, as well as comparable sensitivity and specificity of T1- and T2-weighted sequences in the assessment of adipose tissue, the T2-weighted images were used for the analysis. The cross-section images at height of L2 vertebral body were chosen for segmentation, as this level most accurately reflects the total amount of SAT and VAT in children. The studies of 15 patients were segmented by both observers. Based on obtained data the reproducibility of measurements was assessed by using the Bland-Altman plots. The differences between observers and intra-observer reproducibility were up to 1% for the SAT (mean difference 0.07 cm²) and up to 3% for VAT (mean difference 0.04-0.08 cm²). These results indicated reliability of SAT and VAT measurements for construction of reference values. The sex and age-dependent SAT, VAT and BMI percentile charts were developed based on the lambda-mu-sigma method and LMSChartMaker software. The analysis of the obtained references showed a similar

distribution of BMI percentile lines compared to the available WHO standards. Distribution of SAT percentile lines differed between sexes. In boys, a continuous increase was observed through all age groups (median 66.33 cm² at 18 years of age), while in girls the values stabilized at the age of 14 (median 91.1 cm²). In both sexes, a continuous increase of VAT surface areas was demonstrated in the observed period reaching median of 55.08 cm² in boys and 48.41 cm² in girls at 18 years of age. The distribution of adipose tissue differed between sexes with a predominance of SAT in girls and VAT in boys. The 85th and 95th percentile values on the BMI charts are considered the cut-off points for overweight and obesity. Due to the growing problem of excess body weight in the pediatric population corresponding percentile lines for SAT and VAT were determined.

ii. [Publication 2.](#)

Reference values for MRI-derived psoas and paraspinal muscles and macroscopic fat infiltrations in paraspinal muscles in children.

The second publication aimed to develop tPMA, tPSMA and tMFI reference values in the pediatric population. The study included 465 MR examinations of abdomen, pelvis and lumbar spine of healthy children aged 1 to 18 years (233 girls and 232 boys). The local database was searched for examinations conducted in years 2010-2021 by means of MSD. The examinations of children in the first year of life were excluded from the final analysis due to the insufficient sample size. Semi-automatic tissue segmentation was performed by two observers with the use of pMRI. The PSMA was defined as the sum of multifidus, iliocostalis lumborum, and longissimus muscles. The tPMA, tPSMA, and tMFI represented the sum of muscle areas on both sides of the body. The tMFI surface area was excluded from the tPSMA analysis. Tissue segmentation was performed based on images from standard T2-weighted sequences at level of L4 disc, which correlates well with total muscle mass. If the L4 intervertebral disc was displayed on more than one cross-section, the image closer to the L4 vertebrae body was selected for analysis. The reproducibility of the measurements was assessed by using the Bland-Altman plots based on 40 sets of MR examinations segmented by both observers. The differences between observers and intra-observer reproducibility averaged between 0.39-0.43 cm² for tPMA and 0.05-0.1 cm² for tPSMA. High reproducibility

of segmentation allowed for construction of sex and age-dependent percentile charts based on tPMA, tPSMA and tMFA measurements. The reference values for BMI, weight, muscle and adipose tissue were developed based on the lambda-mu-sigma method using the LMSChartMaker software. The obtained BMI percentile charts were compared with the national reference values (Ola / Olaf study).²⁵⁻²⁶ The population included in the study was characterized by a higher BMI, especially for the +2SD and +1SD ranges (up to 2.7 units in girls and 1.46 units in boys). In the first years of life the distribution of muscle percentile charts was similar in both sexes with subsequent predominance for tPMA and tPSMA in boys from 8 and 10 years of age, respectively. In girls, the flattening of the percentile lines at age of 14 years was noted, reaching median of 26.37 cm² for tPMA and 40.76 cm² for tPSMA at the end of the observed range. Such distribution of percentile charts may be associated with an earlier end of growth phase in female population. In boys, a dynamic increase of tPMA and tPSMA surface areas was observed through all age groups, with corresponding medians of 40.43 cm² and 56.66 cm² at 18 years of age. Compared to the Canadian study based on CT examinations, the 75th, 90th and 95th percentile values showed slightly greater variance, but the overall course of the percentile lines was similar.²¹ The surface area of tMFI in both sexes was comparable from age 1 to 3 years old, with subsequent predominance in girls in the rest of observed range. The mean value of tMFI was consistent with previous studies and reached up to 5% (SD ± 3.65%) in girls and 3.5% (SD ± 2.25%) in boys.

V. SUMMARY

The results of the conducted research enabled construction of MR-derived SAT, VAT, tPMA, tPSMA and tMFI reference values in the pediatric population. The quantitative assessment of adipose and muscle tissue in MR may allow for earlier detection of body composition disorders and personalization of the treatment plan. The widespread use of MR in pediatric standard diagnostic protocols creates the possibility of introducing the proposed method in clinical practice.

BIBLIOGRAFIA / REFERENCES

1. Barlow SE, Dietz WH. Obesity Evaluation and Treatment: Expert Committee Recommendations. *Pediatrics* 1998;102:e29–e29.
2. Fang X, Zuo J, Zhou J, Cai J, Chen C, Xiang E *et al.* Childhood obesity leads to adult type 2 diabetes and coronary artery diseases. *Medicine (Baltimore)* 2019;98:e16825.
3. Barker DJP, Osmond C, Forsén TJ, Kajantie E, Eriksson JG. Trajectories of Growth among Children Who Have Coronary Events as Adults. *N Engl J Med* 2005;353:1802–1809.
4. Suzuki D, Kobayashi R, Sano H, Hori D, Kobayashi K. Sarcopenia after induction therapy in childhood acute lymphoblastic leukemia: its clinical significance. *Int J Hematol* 2018;107:486–489.
5. López JJ, Cooper JN, Albert B, Adler B, King D, Minneci PC. Sarcopenia in children with perforated appendicitis. *J Surg Res* 2017;220:1–5.
6. Dedhia PH, White Y, Dillman JR, Adler J, Jarboe MD, Teitelbaum DH *et al.* Reduced paraspinous muscle area is associated with post-colectomy complications in children with ulcerative colitis. *J Pediatr Surg* 2018;53:477–482.
7. Ooi PH, Thompson-Hodgetts S, Pritchard-Wiart L, Gilmour SM, Mager DR. Pediatric Sarcopenia: A Paradigm in the Overall Definition of Malnutrition in Children? *J Parenter Enter Nutr* 2020;44:407–418.
8. Argilés, J.M.; López-Soriano F. The role of cytokines in cancer cachexia. *Med Res Rev* 1999;19:223–248.
9. Sala A, Rossi E, Antillon F, Molina AL, de Maselli T, Bonilla M *et al.* Nutritional status at diagnosis is related to clinical outcomes in children and adolescents with cancer: A perspective from Central America. *Eur J Cancer* 2012;48:243–252.
10. Blijdorp K, van den Heuvel-Eibrink MM, Pieters R, Boot AM, Delhanty PJD, van der Lely A-J *et al.* Obesity Is Underestimated Using Body Mass Index and Waist-Hip Ratio in Long-Term Adult Survivors of Childhood Cancer. *PLoS One* 2012;7:e43269.
11. Murphy AJ, White M, Elliott SA, Lockwood L, Hallahan A, Davies PS. Body composition of children with cancer during treatment and in survivorship. *Am J Clin Nutr* 2015;102:891–896.
12. Wells JCK. A critique of the expression of paediatric body composition data. *Arch Dis*

Child 2001;85:67–72.

13. Talma H, Chinapaw MJM, Bakker B, HiraSing RA, Terwee CB, Altenburg TM. Bioelectrical impedance analysis to estimate body composition in children and adolescents: a systematic review and evidence appraisal of validity, responsiveness, reliability and measurement error. *Obes Rev* 2013;14:895–905.
14. Ellis KJ, Bell SJ, Chertow GM, Chumlea WC, Knox TA, Kotler DP *et al.* Bioelectrical impedance methods in clinical research: a follow-up to the NIH technology assessment conference. *Nutrition* 1999;15:874–880.
15. Horan M, Gibney E, Molloy E, McAuliffe F. Methodologies to assess paediatric adiposity. *Irish J Med Sci (1971 -)* 2015;184:53–68.
16. Jones KI, Doleman B, Scott S, Lund JN, Williams JP. Simple psoas cross-sectional area measurement is a quick and easy method to assess sarcopenia and predicts major surgical complications. *Color Dis* 2015;17:O20–O26.
17. Akima H, Lott D, Senesac C, Deol J, Germain S, Arpan I *et al.* Relationships of thigh muscle contractile and non-contractile tissue with function, strength, and age in boys with Duchenne muscular dystrophy. *Neuromuscul Disord* 2012;22:16–25.
18. Arpan I, Forbes SC, Lott DJ, Senesac CR, Daniels MJ, Triplett WT *et al.* T 2 mapping provides multiple approaches for the characterization of muscle involvement in neuromuscular diseases: a cross-sectional study of lower leg muscles in 5-15-year-old boys with Duchenne muscular dystrophy. *NMR Biomed* 2013;26:320–328.
19. Tinggaard J, Hagen CP, Christensen AN, Mouritsen A, Mieritz MG, Wohlfahrt-Veje C *et al.* Anthropometry, DXA, and leptin reflect subcutaneous but not visceral abdominal adipose tissue on MRI in 197 healthy adolescents. *Pediatr Res* 2017;82:620–628.
20. Mohammad A, De Lucia Rolfe E, Sleigh A, Kivisild T, Behbehani K, Wareham NJ *et al.* Validity of visceral adiposity estimates from DXA against MRI in Kuwaiti men and women. *Nutr Diabetes* 2017;7:e238–e238.
21. Lurz E, Patel H, Lebovic G, Quammie C, Woolfson JP, Perez M *et al.* Paediatric reference values for total psoas muscle area. *J Cachexia Sarcopenia Muscle* 2020;11:405–414.
22. Lurz E, Patel H, Frimpong RG, Ricciuto A, Kehar M, Wales PW *et al.* Sarcopenia in Children With End-Stage Liver Disease. *J Pediatr Gastroenterol Nutr* 2018;66:222–226.
23. O'Connor M, Ryan J, Foley S. Best single-slice location to measure visceral adipose

- tissue on paediatric CT scans and the relationship between anthropometric measurements, gender and VAT volume in children. *Br J Radiol* 2015;88:20140711.
24. Lee S, Kuk JL, Kim Y, Arslanian SA. Measurement site of visceral adipose tissue and prediction of metabolic syndrome in youth. *Pediatr Diabetes* 2011;12:250–257.
 25. Kułaga Z, Grajda A, Gurzkowska B, Gózdź M, Wojtyło M, Świąder A *et al.* Polish 2012 growth references for preschool children. *Eur J Pediatr* 2013;172:753–761.
 26. Kulaga Z, Litwin M, Tkaczyk M, Rózdżyńska A, Barwicka K, Grajda A *et al.* The height-, weight-, and BMI-for-age of Polish school-aged children and adolescents relative to international and local growth references. *BMC Public Health* 2010;10:109.

PUBLIKACJE WCHODZĄCE W SKŁAD ROZPRAWY DOKTORSKIEJ / MANUSCRIPTS
INCLUDED IN THE DOCTORAL DISSERTATION



MRI-Derived Subcutaneous and Visceral Adipose Tissue Reference Values for Children Aged 6 to Under 18 Years

Kacper Marunowski¹, Dominik Świętoń¹, Włodzimierz Bzyl², Małgorzata Grzywińska³, Mariusz Kaszubowski⁴, Piotr Bandosz^{5,6}, Dmitry Khrichenko⁷ and Maciej Piskunowicz^{1*}

¹ Department of Radiology, Medical University of Gdańsk, Gdańsk, Poland, ² Faculty of Mathematics, Physics and Informatics, University of Gdańsk, Gdańsk, Poland, ³ Department of Human Physiology, Medical University of Gdańsk, Gdańsk, Poland, ⁴ Department of Economic Sciences, Faculty of Management and Economics, Institute of Statistics, Gdansk University of Technology, Gdańsk, Poland, ⁵ Department of Public Health and Policy, University of Liverpool, Liverpool, United Kingdom, ⁶ Department of Prevention and Medical Education, Medical University of Gdańsk, Gdańsk, Poland, ⁷ Division of Body Imaging, Department of Radiology, The Children's Hospital of Philadelphia, Philadelphia, PA, United States

OPEN ACCESS

Edited by:

Lilia Castillo-Martinez,
Instituto Nacional de Ciencias
Médicas y Nutrición Salvador Zubirán
(INCMNSZ), Mexico

Reviewed by:

Norma Ramos-Ibañez,
Universidad Autónoma
Metropolitana, Mexico
Wendy Daniella Rodríguez-García,
National Autonomous University of
Mexico, Mexico

*Correspondence:

Maciej Piskunowicz
maciej.piskunowicz@gumed.edu.pl

Specialty section:

This article was submitted to
Clinical Nutrition,
a section of the journal
Frontiers in Nutrition

Received: 11 August 2021

Accepted: 03 September 2021

Published: 01 October 2021

Citation:

Marunowski K, Świętoń D, Bzyl W,
Grzywińska M, Kaszubowski M,
Bandosz P, Khrichenko D and
Piskunowicz M (2021) MRI-Derived
Subcutaneous and Visceral Adipose
Tissue Reference Values for Children
Aged 6 to Under 18 Years.
Front. Nutr. 8:757274.
doi: 10.3389/fnut.2021.757274

The assessment of body composition in pediatric population is essential for proper nutritional support during hospitalization. However, currently available methods have limitations. This study aims to propose a novel approach for nutrition status assessment and introduce magnetic resonance imaging (MRI)-derived subcutaneous and visceral fat normative reference values. A total of 262 healthy subjects aged from 6 to 18 years underwent MRI examinations and anthropometric measurements. MRI images at the second lumbar vertebrae were used by two radiologists to perform the semi-automatic tissue segmentation. Based on obtained adipose tissue surface areas and body mass index (BMI) scores sex-specific standard percentile curves (3rd, 10th, 25th, 50th, 75th, 90th, 97th) and z-scores were constructed using LMS method. Additionally, 85th and 95th centiles of subcutaneous and visceral adipose tissue were proposed as equivalents of overweight and obesity. Bland-Altman plots revealed an excellent intra-observer reproducibility and inter-observer agreement. In conclusion, our findings demonstrate highly reproducible method and suggest that MRI-derived reference values can be implemented in clinical practice.

Keywords: subcutaneous adipose tissue (SAT), visceral adipose tissue (VAT), magnetic resonance imaging, nutritional assessment, age and sex dependent reference values, percentile charts, children

INTRODUCTION

Childhood overweight and obesity have been recognized as strong risk factors for the development of cardiovascular disease, diabetes mellitus, depression, and cancer in adulthood (1, 2). Thus, determining body tissue composition, particularly visceral, and subcutaneous adipose tissue compartments can be useful for the assessment of patient risk stratification. A proper development during the growth period requires an appropriate nutritional status, mainly in children with coexisting chronic cardiovascular or oncological diseases (3, 4). In routine clinical practice, the assessment of obesity grade and body fat content is based on anthropometric measures and indexes such as skinfold thickness, body mass index (BMI), or waist to hip ratio (WtHR) in comparison

to the healthy population. Currently, body impedance analysis (BIA), which enables algorithm-based estimation of adipose and lean body mass has been increasingly used. While these methods are convenient and accessible in clinical routine practice, their accuracy in reflecting malnutrition and capability to differentiate visceral adipose tissue (VAT) and subcutaneous adipose tissue (SAT) compartments are limited (5–7). Anthropometric measurements tend to underestimate the incidence of obesity and malnutrition, especially with the coexistence of disease both during the initial assessment and over the longer-term following the treatment (8, 9). BIA is safe and demonstrates higher sensitivity than anthropometric methods, but underestimates the amount of adipose tissue in lean children and overestimates in obese ones (5). Although there are imaging methods including dual-energy x-ray absorptiometry (DXA) and computed tomography (CT) which directly discern body compartments with high accuracy, their role in the pediatric population is limited due to the radiation burden (10–12). Another diagnostic tool frequently used in children is magnetic resonance imaging (MRI). Due to the different magnetic properties of water and fat-bound protons, this radiation-free technique allows to assess lean and adipose tissue compartments (13–17). However, a dedicated MRI whole-body protocol for the assessment of nutritional status is highly costly and time-demanding thus is limited in clinical use. In this context, it seems crucial to establish a simple and fast method of VAT and SAT quantification using MRI which can be obtained during the regular diagnostic protocol. A method that meets these requirements was already validated in adult population fat quantification from a single CT and MRI slice at the L2-L3 vertebral level (18–22). With this approach, all adipose tissue measurements can be obtained from routine diagnostic protocol with high correlation to MRI whole-body examination adipose tissue volumes.

Considering the limitation of currently available methods, this study aimed to establish the gender-dependent reference normative values of MRI-derived visceral and subcutaneous adipose tissue in a healthy pediatric population, which can serve as reference standards in the evaluation of body composition in children and adolescence with nutrition disorders.

MATERIALS AND METHODS

Patients

This retrospective study was approved by the Institutional Ethics Committee the approved number of our project is NKBBN/443/2018. Eligible participants were children and adolescence aged 0–18 who underwent MRI examination of the abdomen or pelvis in the years 2010–2020. The local database was searched by use of the dedicated search engine MedStream Designer (MSD) and 1,315 records were found. Exclusion criteria included incorrect search by MSD (281), examinations without T2-weighted sequences (48), T2-weighted sequences distorted by artifacts (47), a history of oncological or hematological disease, hydronephrosis, ascites, glycogen storage diseases (520), patients post nephrectomy, or other surgical procedure (59). The remaining 24 MRI records were follow up studies thus

were excluded from the analysis (23). The MRI examinations of children aged 0–5 were also excluded due to insufficient sample size (74). The final analysis included a total of 262 children or adolescence aged 6–18 years (111 girls, and 151 boys) without changes or with changes of benign origin.

Demographic Characteristics

Demographic characteristics included patients' age, weight, and height at time of MRI examination. BMI was calculated for each subject by dividing weight in kilograms by square of the height in meters.

Imaging Method

Three different MRI systems were used: two 1.5T systems Magnetom Aera and Magnetom Sola (Siemens Healthineers, Erlangen, Germany) and one 3.0T system Philips Achieva 3.0 TX (Philips Medical Systems Netherlands, Best, Netherlands). MRI examinations of the abdomen and/or pelvis were performed by using the standard protocols. A standard TSE T2-weighted sequence in the transverse plane was taken for analysis. A single slice at the level of the second lumbar vertebra was selected for visceral and subcutaneous adipose tissue evaluation.

Adipose Tissue Quantification

The fat tissue compartment was segmented into SAT and VAT. The SAT was defined as subcutaneous fat externally of the abdominal and back muscles. The VAT was defined as adipose tissue inside of the abdominal cavity, excluding fat depots within abdominal and back muscles and fat tissue extending beyond the posterior outline of the vertebral body. Both arms visible on the analysis page were excluded from adipose tissue quantification.

Semi-automatic body composition analysis was performed with the use of parametric Magnetic Resonance Imaging v1.2.31-b (pMRI) software. The program is freeware available at the website www.parametricmri.com. The T2-weighted sequence was loaded into pMRI and processed with the volumetric region of interest analysis module which allows for segmentation and volumetric quantification of adipose tissues. A single slice at the level of the second lumbar vertebra was selected for the assessment of adipose tissue. For the analysis of SAT and VAT signal intensity, thresholds were manually set. After signal intensity-based segmentation, all data sets were visually revised (**Figure 1**). Misclassified tissues were corrected by two operators. One hundred seventy-two sets by KM (2nd year of specialization in radiology) and ninety sets by MP (radiologist with 15 years of experience in MRI). The average time needed for analysis and correction of a single data set was ~between 5 and 15 min. The example of segmented cross-section is presented in **Figure 1**.

Statistical Analysis

Statistical Analysis of MRI Images

Agreement of segmentation results between observers and intra-observer reproducibility were assessed by using the Bland-Altman plots. The limits of agreement of the Bland-Altman plots were defined as the mean differences $\pm 90\%$ confidence intervals. Statistical analysis was performed in R version 4.1.0.

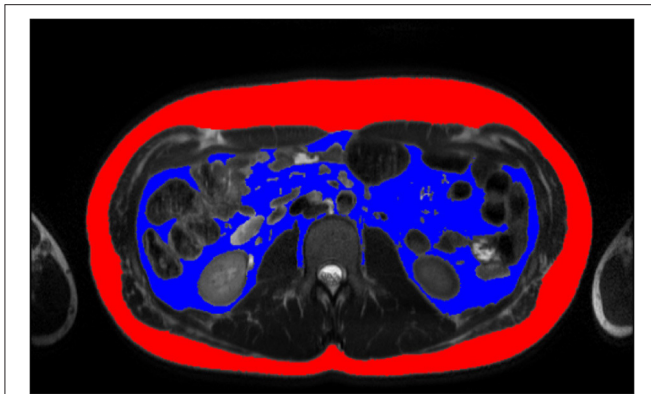


FIGURE 1 | Example of tissue SAT (red) and VAT (blue) segmentation of 14 years old boy, BMI: 27.7 kg/m² by MP. BMI, Body Mass Index, MP, second radiologist; SAT, subcutaneous adipose tissue; VAT, visceral adipose tissue.

Statistical Analysis of Percentile Charts

Sex-specific BMI-for-age, SAT-for-age and VAT-for-age percentile curves and z-scores were constructed using the lambda-mu-sigma (LMS) method (24) and LMSChartMaker Light version 2.54 software (23). Identification of outliers was made by inspecting the z-score plot of each variable. None of the outliers were considered to be made due to mistakes of data recording or transferring. Following WHO guidelines (25, 26), derivation of percentiles was enabled only within the interval of z-scores between -3.0 and 3.0 . To avoid assumptions about the distribution of data beyond the limits of observed values, the standard deviation at each age beyond this limit was fixed at the distance -2.5 SD and 2.5 SD correspondingly. In boys four SAT, three VAT, and one BMI values were fixed; in girls-only one SAT, two VAT, and one BMI values were fixed.

The LMS is based on the assumption that by use of Box-Cox transformation any anthropometric data such as BMI can be converted to a normal distribution for any given age (age was used as a continuous variable). Natural cubic splines with knots at each distinct age t were fitted to create three smooth curves representing the skewness $L(t)$ [Box-Cox transformation], the median $M(t)$, and the coefficient of variation $S(t)$ of the original data as they vary with age:

$$C\alpha(t) = M(t) \times [1 + L(t) \times S(t) \times Z\alpha]^{1/L(t)}$$

where $Z\alpha$ is the α -quantile of a standard normal distribution and $C\alpha(t)$ is a percentile corresponding to $Z\alpha$. Equivalent degrees of freedom (edf) $L(t)$, $M(t)$, and $S(t)$ measure the complexity of each fitted curve. In our limited sample size, for each data set the standard edf of L3, M5, S3 was chosen, as further fitting made no significant improvements to our model (23).

RESULTS

The inter-observer agreement was assessed based on 15 sets of randomly selected MRI examinations segmented separately by both radiologists (KM and MP) (**Supplementary Figures 1, 2**).

The same set of images was subsequently resegmented by one radiologist (K.M.) for the evaluation of the intra-observer reproducibility. Results in form of Bland-Altman plots are presented in the supplementary material (**Supplementary Figures 3, 4**). For SAT both intra- and inter-observer mean differences were at the level of 0.07 cm². The actual differences were up to 2 cm² for intra- and 0.5 cm² for inter-observer measurements which represents disagreement at a level of 1% for corresponding measurements. Slightly higher intra- and inter-observer disagreement was noted in VAT segmentation reaching accordingly up to 2.4 cm² (mean -0.04 cm²) and 2.7 cm² (mean 0.08 cm²). In those cases maximum difference in measurements was around 3%.

For the adjustment of BMI-for-age, SAT-for-age, and VAT-for-age percentiles the 262 MRI pediatric examinations (111 girls, and 151 boys) aged 6–18 (mean age of 12.49 years) were enrolled. The SAT and VAT reference values in each age group for boys and girls are presented in **Tables 1–4**. Based on the results percentile curves for SAT and VAT were calculated and presented in **Figures 2–5**.

Corresponding BMI growth charts are presented in the supplementary material in correlation to age (**Supplementary Figures 5, 6**). Among both genders, BMI increased continuously during childhood and adolescence, reaching a median of 22.5 kg/m² in boys and 21.7 kg/m² in girls at the end of the observed age range (18 years). In the groups between 8 and 10 years old, the flattening of the centile curves for BMI was observed, especially noticeable in the percentile range from 3 to 50.

The distribution of SAT percentiles were different between both genders. In boys, a continuous increase was observed throughout all age groups, reaching the median of 66.33 cm² at 18 years of age. In girls, at the beginning of maturity-onset (from age 7 to 11 years), a dynamic increase of SAT surface area was noted, which then stabilized at the age of 14 years (median of 91.1 cm²).

For SAT, the difference between the 3rd and 97th percentile reached a maximum of 307.85 cm² for boys 12 years of age, while the maximum difference for girls (287.54 cm²) was attained at 13 years of age (**Tables 1, 2**).

The distribution of VAT percentiles was comparable for both genders. Both boys and girls showed a continuous increase in surface areas in all age groups, reaching the median of 55.08 cm² in boys and 48.41 cm² in girls at 18 years of age, respectively.

The difference of VAT areas between extreme percentiles increased continuously until age of 12 years in girls and until the end of the observed age range in boys. At this age, the difference of 81.15 and 137.14 cm², respectively, was attained, however in girls from 11 years onwards no substantial differences were noted (**Tables 3, 4**).

DISCUSSION

This the first study which demonstrates the reference values of the subcutaneous and visceral adipose tissue as the percentile charts for girls and boys from 6 to 18 years of age.

TABLE 1 | SAT-for-age (cm²) references for boys.

Age (years)	-2 SD	-1SD	1 SD	2 SD	P3	P5	P10	P25	P50	P75	P85	P90	P95	P97
6	12.59	16.65	32.90	50.62	13.00	13.86	15.34	18.37	22.84	29.03	33.38	36.86	43.04	47.88
7	11.93	17.64	47.90	94.22	12.47	13.63	15.71	20.29	27.80	39.65	48.96	57.03	72.69	86.13
8	12.37	20.17	71.96	174.74	13.07	14.60	17.45	24.06	35.83	56.40	74.04	90.25	123.97	155.09
9	13.82	23.94	100.41	274.09	14.69	16.64	20.33	29.19	45.72	76.26	103.69	129.70	185.76	239.42
10	15.10	27.26	123.36	342.98	16.13	18.45	22.89	33.69	54.22	92.71	127.52	160.58	231.70	299.44
11	15.53	28.92	135.35	368.56	16.66	19.20	24.08	36.05	58.90	101.63	139.91	175.90	252.16	323.41
12	15.35	29.27	139.05	367.50	16.52	19.15	24.23	36.72	60.54	104.67	143.67	179.89	255.33	324.37
13	15.12	29.39	140.52	360.87	16.31	19.00	24.21	37.04	61.42	106.13	145.11	180.88	254.24	320.19
14	15.04	29.69	142.40	357.15	16.26	19.02	24.37	37.55	62.53	107.89	146.98	182.51	254.45	318.21
15	15.04	30.07	144.48	355.74	16.29	19.12	24.61	38.13	63.70	109.76	149.07	184.53	255.64	317.96
16	15.06	30.43	146.40	355.33	16.34	19.23	24.84	38.67	64.76	111.45	151.01	186.47	257.04	318.37
17	15.08	30.72	147.97	355.13	16.38	19.32	25.03	39.12	65.63	112.84	152.59	188.07	258.23	318.79
18	15.09	30.95	149.23	354.93	16.40	19.38	25.18	39.47	66.33	113.95	153.86	189.33	259.14	319.09

P, percentile; SAT, subcutaneous adipose tissue; SD, standard deviation.

TABLE 2 | SAT-for-age (cm²) references for girls.

Age (years)	-2 SD	-1SD	1 SD	2 SD	P3	P5	P10	P25	P50	P75	P85	P90	P95	P97
6	15.01	18.77	34.93	56.73	15.38	16.18	17.55	20.38	24.64	30.84	35.44	39.33	46.70	52.96
7	13.94	21.32	61.34	121.92	14.62	16.11	18.81	24.79	34.69	50.41	62.75	73.41	93.97	111.47
8	18.75	33.82	118.62	231.60	20.09	23.06	28.58	41.20	62.52	96.01	121.48	142.78	181.99	213.50
9	19.40	37.72	141.25	271.92	21.00	24.57	31.29	46.81	73.12	114.04	144.67	169.91	215.57	251.54
10	20.97	41.60	158.17	303.46	22.77	26.78	34.34	51.86	81.57	127.65	162.00	190.22	241.06	280.94
11	22.57	44.82	170.59	237.12	24.51	28.83	36.99	55.90	87.96	137.68	174.72	205.14	259.92	302.87
12	23.37	46.34	175.94	337.23	25.38	29.84	38.26	57.75	90.80	142.03	180.19	211.54	267.98	312.23
13	23.59	46.67	176.64	338.17	25.61	30.10	38.56	58.14	91.30	142.66	180.90	212.30	268.83	313.15
14	23.64	46.66	176.02	336.58	25.65	30.13	38.57	58.09	91.11	142.22	180.26	211.48	267.68	311.72
15	23.60	46.53	175.01	334.14	25.61	30.07	38.48	57.89	90.72	141.47	179.21	210.18	265.88	309.52
16	23.57	46.43	174.20	332.08	25.57	20.03	38.41	57.75	90.42	140.88	178.37	209.12	264.39	307.67
17	23.59	46.43	173.82	330.93	25.59	30.04	38.41	57.73	90.33	140.64	177.98	208.59	263.60	306.65
18	23.63	46.47	173.69	330.31	25.63	30.08	38.46	57.77	90.35	140.57	177.84	208.37	263.22	306.12

P, percentile; SAT, subcutaneous adipose tissue; SD, standard deviation.

Currently, the importance of adequate nutritional status during illness is strongly emphasized. Over the years a wide variety of VAT metabolic activity was confirmed highlighting the importance of the body composition assessment during treatment (27–29). Volume and distribution of adipose tissues determine the type and intensity of malnutrition and therefore enable adequate nutritional support (30, 31).

Appropriate assessment of VAT in the pediatric population is considered to be a serious problem. Most of currently available measurement methods have limitations as discussed in the introduction (8, 9). In contrast, MRI enables direct, accurate, quantitative assessment of all compartments of body fat and is a radiation-free technique which allows safe and long-term observation in body composition changes during growth when compared to CT.

Our study plan was to use the safest method with high efficiency in the quantitative assessment of VAT and SAT. This can be done with MRI imaging which is a commonly used technique in pediatric population during the routine diagnostic process. The accuracy and reproducibility of the MRI examination in the assessment of adipose tissue have already been proved in both adult and pediatric patients (14, 32). The semi-automatic methodology used in our study is consistent with previous studies. In our study, SAT and VAT surface area results obtained by both radiologists on slices at the level of second lumbar vertebrae of randomly selected patients showed high intra-observer reproducibility and inter-observer agreement (**Supplementary Figures 1–4**). Both in SAT and VAT plots, the mean difference between radiologists was insignificant up to 2.5 cm² indicating that one of them selected larger areas as adipose

TABLE 3 | VAT-for-age (cm²) references for boys.

Age (years)	-2 SD	-1SD	1 SD	2 SD	P3	P5	P10	P25	P50	P75	P85	P90	P95	P97
6	13.00	19.35	31.61	37.60	13.77	15.28	17.58	21.38	25.54	29.65	31.38	33.31	35.48	36.89
7	12.38	20.06	43.99	61.09	13.16	14.82	17.64	23.13	30.46	39.22	44.55	48.42	54.58	58.85
8	13.60	21.46	53.64	84.95	14.36	15.99	18.87	24.91	33.91	46.20	54.55	61.05	72.15	80.42
9	16.56	25.87	68.35	116.36	17.44	19.35	22.76	30.07	41.46	57.89	69.64	79.12	95.95	109.01
10	18.53	28.76	77.50	136.57	19.50	21.58	25.33	33.42	46.23	65.17	79.04	90.41	110.97	127.27
11	19.97	30.68	82.99	149.33	20.97	23.16	27.08	35.59	49.18	69.55	84.69	97.22	120.21	138.69
12	20.74	31.57	85.23	155.52	21.76	23.96	27.93	36.55	50.37	71.29	86.99	100.10	124.36	144.08
13	21.29	32.16	86.46	159.30	22.31	24.52	28.50	37.16	51.07	72.25	88.26	101.70	126.77	147.32
14	21.87	32.82	87.88	163.08	22.90	25.13	29.13	37.86	51.91	73.40	89.72	103.49	129.30	150.60
15	22.45	33.52	89.44	166.92	23.49	25.74	29.79	38.61	52.84	74.67	91.32	105.41	131.95	153.97
16	22.98	34.17	90.91	170.48	24.03	26.31	20.40	39.32	53.72	75.87	92.83	107.22	134.44	157.11
17	23.43	34.72	92.17	173.53	24.49	26.79	30.92	39.92	54.47	76.90	94.12	108.77	136.56	159.79
18	23.80	35.18	93.21	176.05	24.87	27.19	31.35	40.42	55.08	77.75	95.18	110.04	138.30	162.01

P, percentile; SD, standard deviation; VAT, visceral adipose tissue.

TABLE 4 | VAT-for-age (cm²) references for girls.

Age (years)	-2 SD	-1SD	1 SD	2 SD	P3	P5	P10	P25	P50	P75	P85	P90	P95	P97
6	14.83	20.56	36.84	47.88	15.44	16.70	18.80	22.75	27.82	33.69	37.20	39.73	43.71	46.45
7	15.15	20.94	42.31	62.16	15.74	16.97	19.08	23.35	29.46	37.52	42.89	47.03	54.07	59.29
8	17.92	24.76	54.25	88.73	18.59	20.02	22.52	27.75	35.68	47.01	55.15	61.79	73.77	83.29
9	19.15	26.40	58.89	99.56	19.85	21.36	24.01	29.59	38.18	50.71	59.91	67.53	81.56	92.95
10	20.90	28.88	63.92	106.31	21.68	23.34	26.26	32.37	41.71	55.21	65.01	73.07	87.74	99.52
11	22.40	31.12	68.38	111.08	23.25	25.07	28.27	34.92	44.98	59.29	69.51	77.80	92.67	104.40
12	22.89	32.03	70.12	111.84	23.79	25.70	29.05	35.99	46.39	60.98	71.25	79.49	94.09	105.44
13	22.81	32.13	70.24	110.56	23.73	25.68	29.09	36.15	46.65	61.21	71.35	79.42	93.58	104.47
14	22.73	32.19	70.38	109.79	23.67	25.65	29.11	36.26	46.85	61.41	71.48	79.44	93.31	103.89
15	22.77	32.38	70.81	109.79	23.72	25.73	29.26	36.50	47.21	61.85	71.91	79.83	93.57	104.00
16	22.87	32.63	71.38	110.18	23.83	25.88	29.46	36.81	47.64	62.38	72.48	80.40	94.09	104.44
17	22.98	32.88	71.93	110.66	23.96	26.04	29.66	37.11	48.05	62.90	73.03	80.97	94.64	104.95
18	23.08	33.09	72.42	111.09	24.07	26.17	29.84	37.37	48.41	63.35	73.52	81.47	95.13	105.42

P, percentile; SD, standard deviation; VAT, visceral adipose tissue.

tissue. In both intra- and inter-observer Bland-Altman plots, greater differences between measurements were noted in VAT groups. However, actual differences in measured adipose tissue areas were up to 2.5 cm², which makes this difference almost negligible. The high correlation between observers obtained in our study indicates the reliability of SAT and VAT measurements suggesting that these findings can be used to build models of the percentile charts.

Considering the purpose of our study and pediatric population, we had to change the current MRI image sequence approach which is commonly used for adipose tissue quantification. To date, the majority of published studies have used T1-weighted water-fat sequences (called Dixon sequence). While these sequences have a short acquisition time, the quality of acquired images are strongly dependent on the

ability to breath-hold during the examination. The sufficiently long breath-hold is difficult for young children and impossible in case of sedation. Thus, Dixon images of abdomen and pelvis acquired in children are frequently burdened by movement artifacts, making this impossible to evaluate the change in body composition (33). To overcome this limitation, our study used T2-weighted sequences. In the study of Pescatori et al. has shown that the sensitivity and specificity of T1- and T2-weighted sequences in the assessment of adipose tissue are comparable but the results of T2-weighted sequences tended to be more reproducible (32). Furthermore, T2-weighted sequences are included in all standard examination protocols of the abdominal and/or pelvis cavity. Thus, utilizing these sequences for the assessment of SAT and VAT has no major impact on examination and sedation time

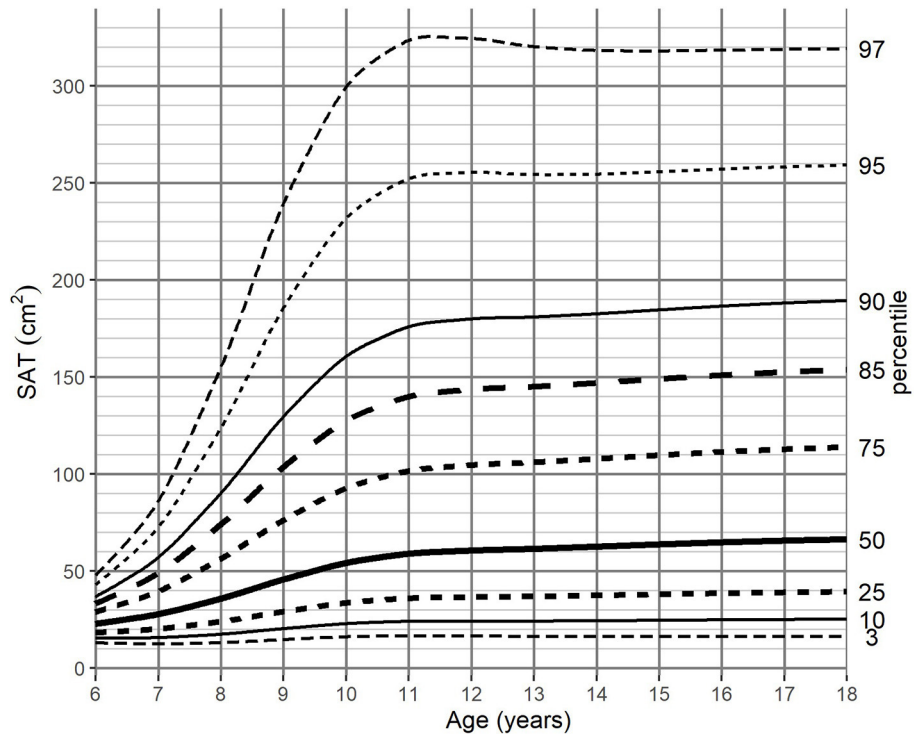


FIGURE 2 | SAT-for-age (cm²) percentile charts for boys aged from 6 to 18 years. SAT, subcutaneous adipose tissue.

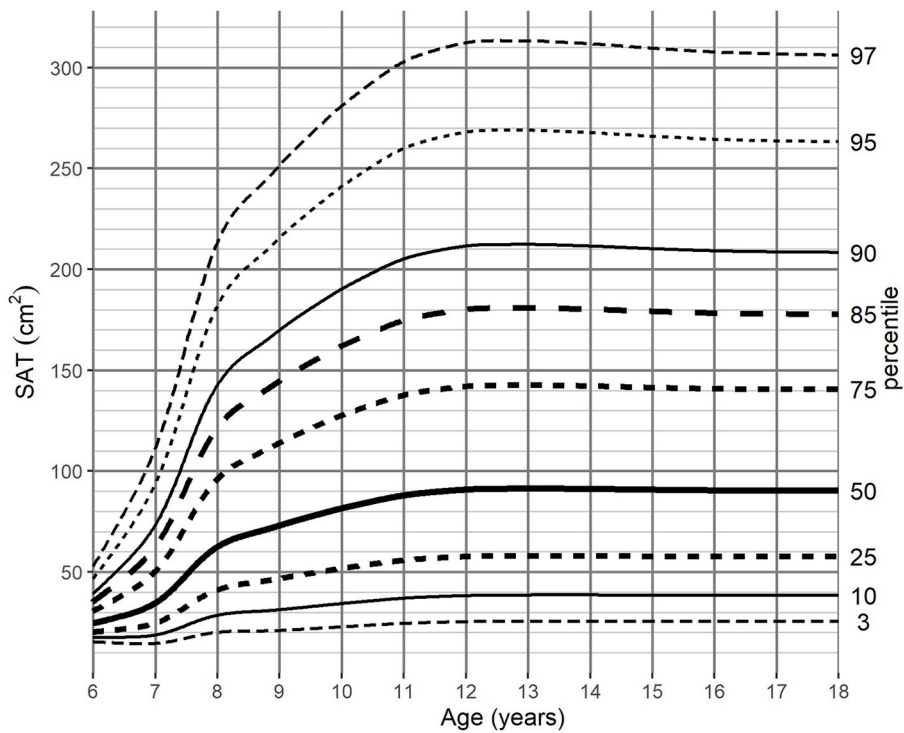
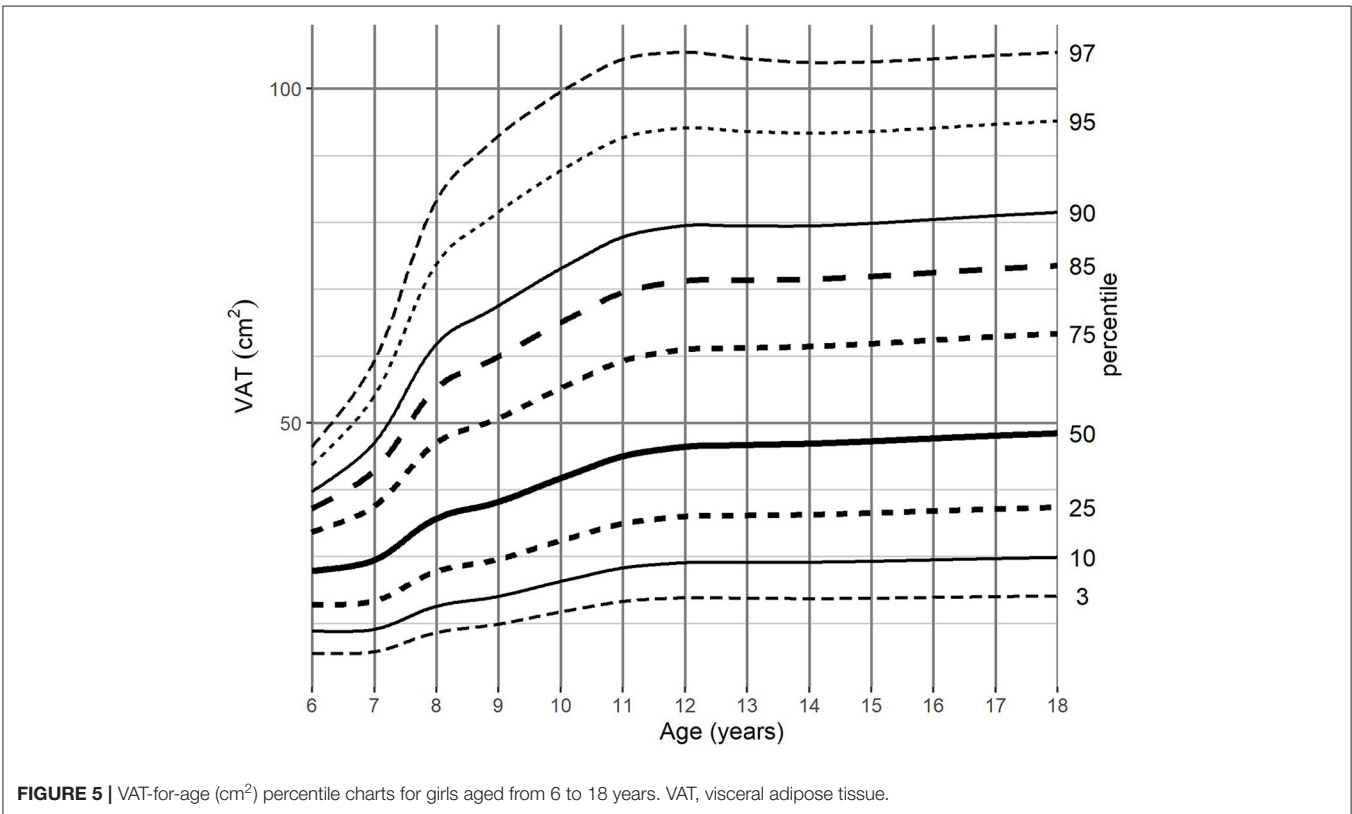
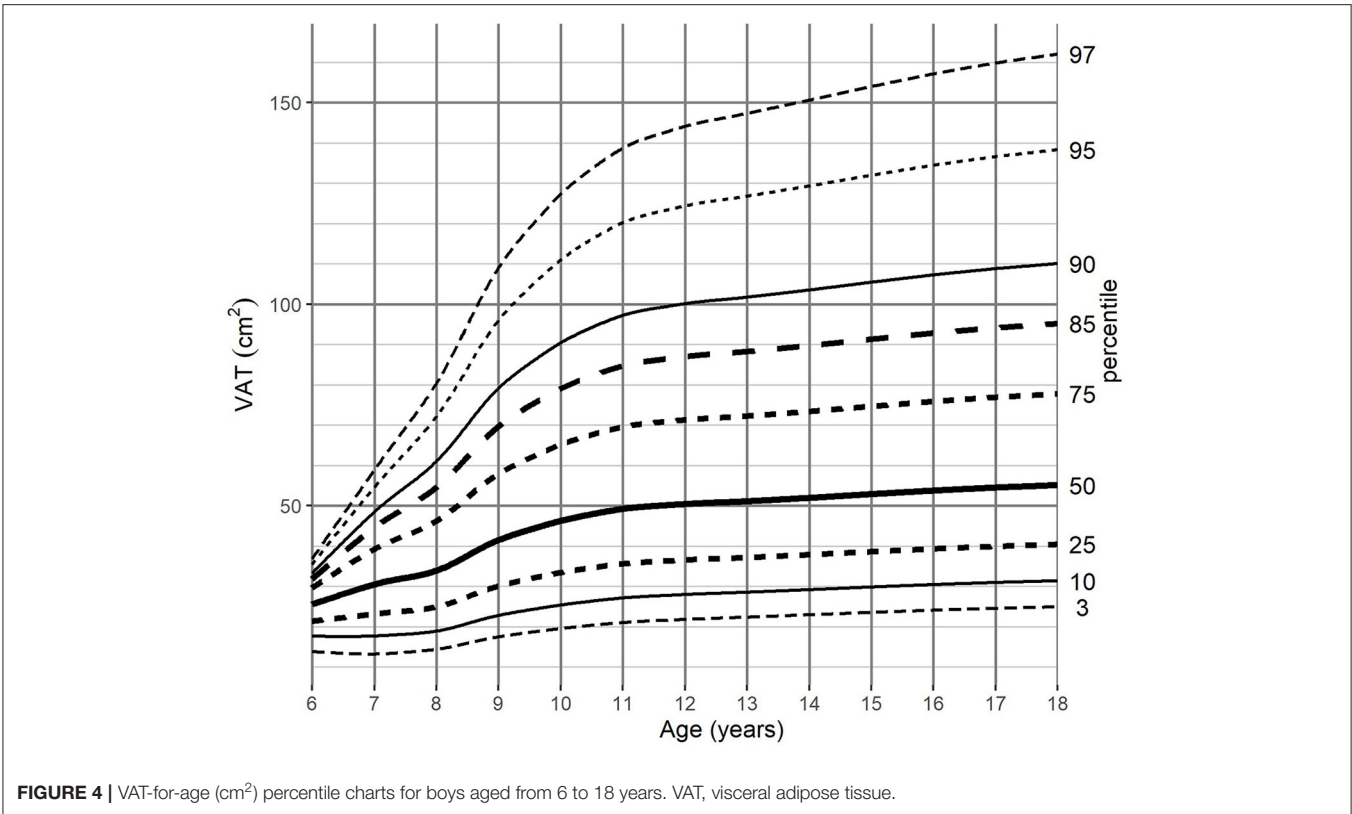


FIGURE 3 | SAT-for-age (cm²) percentile charts for girls aged from 6 to 18 years. SAT, subcutaneous adipose tissue.



Proper assessment of obtained images requires the involvement of highly qualified personnel. Although tools for manual or semi-automatic SAT and VAT quantification are widely available, segmentation throughout all slices at the level of abdominal or pelvis cavities is time-consuming and impractical (34). Therefore, the quantity of particular adipose tissue depots is usually estimated based on a single cross-section image (18–22, 35, 36). According to the current knowledge, in children cross-sections at the height of L2 vertebrae are the most accurate and correlate to the total amount of SAT and VAT (35, 36). Although in the future artificial intelligence (AI) algorithms may simplify the adipose tissue segmentation process, the current utilization of the single-slice approach is the most optimal solution.

In this context, in the present study by creating the SAT and VAT percentile charts we provide a tool that can be widely and easily implemented in clinical practice. The percentile charts are costless, easy, quick to apply, and enable observation of the growth tendencies over the longer term. The most used percentile charts in pediatric populations are weight, height, and BMI charts (37). However, BMI percentile curves are created by averaging not only SAT and VAT, but also muscle and internal organs mass. As a result, the BMI percentile charts cannot properly illustrate changes in the adipose tissue during children's growth (6, 38). Regardless of gender, the BMI values presented a continuous increase from 6 to 18 years of age both in data presented by WHO (39), as well as in our study. However, only the value of VAT showed a similar upward trend. The SAT surface area stabilized around the age of 12 for both boys and girls. The distribution of BMI standard deviations scores in our population was similar to the regional reference values (40). However, flattening of the BMI curves in the age range from 8 to 10 years in both sexes was noticeable which may be related to the size of our study group.

It should be emphasized that in the same age range, in the contrary to BMI, the SAT, and VAT percentile curves showed a continuous increase. These findings may indicate that our method is more sensitive and precise at reflecting the actual changes in the amount and distribution of body fat.

In our study, data from children with known disorders affecting growth were excluded. The presented standard deviation scores and percentiles should be considered as growth references (not growth standards according to the WHO terminology) because we did not identify environmental conditions “likely to favor the achievement of children's full genetic growth potential” (25). To better monitor, the growing problem of overweight and obesity among children and adolescents in the recommendations of the pediatric obesity experts committee the cut-off values have been determined at the level of 85th and 95th percentiles as the best equivalents of adults' 25th and 30th BMI values (41). Similarly, in our study for the SAT and VAT percentile charts, we proposed the 85th and 95th percentile curves as warning points, above which attention for overweight is required. Determining the exact percentile cut-off for SAT and VAT overweight and obesity requires further research on a larger population.

This study has several limitations. Firstly, the number of participants was relatively small, as percentile charts are usually created during population-based prospective studies. Our study was conducted at a single-center, therefore our results only refer to the Caucasian population. Additionally, semi-automatic adipose tissue assessment is time-consuming and further research on a larger study group would require the implementation of fully automatic tools based on AI deep learning algorithms. Further limitation of this study is the lack of centile charts for children from birth to 5 years of age. Since percentile charts for the youngest children are commonly presented in monthly intervals, our study did not include a sufficient number of healthy participants in these age groups to obtain reliable results.

In conclusion, for the first time, we have shown reference values of SAT and VAT in form of percentile charts for boys and girls during childhood and adolescence. Frequent utilization of MRI examinations in the pediatric population may enable the implementation of our method in clinical practice for body composition assessment and proper nutritional support. In the view of the rapid development of AI deep learning algorithms, there seems to be a high possibility of automatization and incorporation of MRI-based adipose tissue assessment into standard diagnostic protocols.

DATA AVAILABILITY STATEMENT

The datasets presented in this article are not readily available because the need of agreement from University Clinical Center of Gdańsk. Requests to access the datasets should be directed to mleszczynska@uck.gda.pl.

ETHICS STATEMENT

The studies involving human participants were reviewed and approved by Independent Bioethics Committee for Scientific Research at Medical University of Gdańsk. Written informed consent to participate in this study was provided by the participants' legal guardian/next of kin.

AUTHOR CONTRIBUTIONS

KM and MP contributed to the conception or design of the work and drafted the manuscript. KM, WB, MG, MK, PB, DK, and MP contributed to the acquisition, analysis, or interpretation of data for the work. DS, WB, DK, and MG critically revised the manuscript. All authors gave final approval and agree to be accountable for all aspects of work ensuring integrity and accuracy.

SUPPLEMENTARY MATERIAL

The Supplementary Material for this article can be found online at: <https://www.frontiersin.org/articles/10.3389/fnut.2021.757274/full#supplementary-material>

REFERENCES

- Fang X, Zuo J, Zhou J, Cai J, Chen C, Xiang E, et al. Childhood obesity leads to adult type 2 diabetes and coronary artery diseases. *Medicine*. (2019) 98:e16825. doi: 10.1097/MD.00000000000016825
- Barker DJP, Osmond C, Forsén TJ, Kajantie E, Eriksson JG. Trajectories of growth among children who have coronary events as adults. *N Engl J Med*. (2005) 353:1802–9. doi: 10.1056/NEJMoa044160
- Co-Reyes E, Li R, Huh W, Chandra J. Malnutrition and obesity in pediatric oncology patients: causes, consequences, and interventions. *Pediatr Blood Cancer*. (2012) 59:1160–7. doi: 10.1002/pbc.24272
- Bauer J, Jürgens H, Frühwald MC. Important aspects of nutrition in children with cancer. *Adv Nutr*. (2011) 2:67–77. doi: 10.3945/an.110.000141
- Talma H, Chinapaw MJM, Bakker B, HiraSing RA, Terwee CB, Altenburg TM. Bioelectrical impedance analysis to estimate body composition in children and adolescents: a systematic review and evidence appraisal of validity, responsiveness, reliability and measurement error. *Obes Rev*. (2013) 14:895–905. doi: 10.1111/obr.12061
- Wells JC. A Hattori chart analysis of body mass index in infants and children. *Int J Obes Relat Metab Disord*. (2000) 24:325–9. doi: 10.1038/sj.ijo.0801132
- Mulasi U, Kuchnia AJ, Cole AJ, Earthman CP. Bioimpedance at the bedside: current applications, limitations, and opportunities. *Nutr Clin Pract*. (2015) 30:180–93. doi: 10.1177/0884533614568155
- Murphy AJ, White M, Elliott SA, Lockwood L, Hallahan A, Davies PS. Body composition of children with cancer during treatment and in survivorship. *Am J Clin Nutr*. (2015) 102:891–6. doi: 10.3945/ajcn.114.099697
- Blijdorp K, van den Heuvel-Eibrink MM, Pieters R, Boot AM, Delhanty PJD, van der Lely AJ, et al. Obesity is underestimated using body mass index and waist-hip ratio in long-term adult survivors of childhood cancer. *PLoS ONE*. (2012) 7:e43269. doi: 10.1371/journal.pone.0043269
- Horan M, Gibney E, Molloy E, McAuliffe F. Methodologies to assess paediatric adiposity. *Irish J Med Sci*. (2015) 184:53–68. doi: 10.1007/s11845-014-1124-1
- Zemel BS. Quantitative computed tomography and computed tomography in children. *Curr Osteoporos Rep*. (2011) 9:284–90. doi: 10.1007/s11914-011-0076-x
- Huang TT, Johnson MS, Figueroa-Colon R, Dwyer JH, Goran MI. Growth of visceral fat, subcutaneous abdominal fat, and total body fat in children. *Obesity*. (2001) 9:283–9. doi: 10.1038/oby.2001.35
- Simoni P, Guglielmi R, Gómez MPA. Imaging of body composition in children. *Quant Imaging Med Surg*. (2020) 10:1661–71. doi: 10.21037/qims.2020.04.06
- Tinggaard J, Hagen CP, Christensen AN, Mouritsen A, Mieritz MG, Wohlfahrt-Veje C, et al. Anthropometry, DXA, and leptin reflect subcutaneous but not visceral abdominal adipose tissue on MRI in 197 healthy adolescents. *Pediatr Res*. (2017) 82:620–8. doi: 10.1038/pr.2017.138
- Gaeta M, Scribano E, Mileto A, Mazziotti S, Rodolico C, Toscano A, et al. Muscle fat fraction in neuromuscular disorders: dual-echo dual-flip-angle spoiled gradient-recalled MR imaging technique for quantification—a feasibility study. *Radiology*. (2011) 259:487–94. doi: 10.1148/radiol.10101108
- Baum T, Cordes C, Dieckmeyer M, Ruschke S, Franz D, Hauner H, et al. MR-based assessment of body fat distribution and characteristics. *Eur J Radiol*. (2016) 85:1512–8. doi: 10.1016/j.ejrad.2016.02.013
- Idilman IS, Keskin O, Celik A, Savas B, Halil Elhan A, Idilman R, et al. A comparison of liver fat content as determined by magnetic resonance imaging-proton density fat fraction and MRS versus liver histology in non-alcoholic fatty liver disease. *Acta Radiol*. (2016) 57:271–8. doi: 10.1177/0284185115580488
- Shen W, Punyanitya M, Chen J, Gallagher D, Albu J, Pi-Sunyer X, et al. Visceral adipose tissue: relationships between single slice areas at different locations and obesity-related health risks. *Int J Obes*. (2007) 31:763–9. doi: 10.1038/sj.ijo.0803474
- Irlbeck T, Massaro JM, Bamberg F, O'Donnell CJ, Hoffmann U, Fox CS. Association between single-slice measurements of visceral and abdominal subcutaneous adipose tissue with volumetric measurements: the Framingham Heart Study. *Int J Obes*. (2010) 34:781–7. doi: 10.1038/ijo.2009.279
- Maislin G, Ahmed MM, Gooneratne N, Thorne-Fitzgerald M, Kim C, Teff K, et al. Single slice vs. volumetric MR assessment of visceral adipose tissue: reliability and validity among the overweight and obese. *Obesity*. (2012) 20:2124–32. doi: 10.1038/oby.2012.53
- Kuk JL, Church TS, Blair SN, Ross R. Measurement site and the association between visceral and abdominal subcutaneous adipose tissue with metabolic risk in women. *Obesity*. (2010) 18:1336–40. doi: 10.1038/oby.2009.414
- Kuk JL, Church TS, Blair SN, Ross R. Does measurement site for visceral and abdominal subcutaneous adipose tissue alter associations with the metabolic syndrome? *Diabetes Care*. (2006) 29:679–84. doi: 10.2337/diacare.29.03.06.dc05-1500
- LMSchartmaker Light | Health for all Children. Available online at: <https://www.healthforallchildren.com/shop-base/shop/software/lmschartmaker-light/> (accessed: Jun 6, 2021).
- Cole TJ. The LMS method for constructing normalized growth standards. *Eur J Clin Nutr*. (1990) 44:45–60.
- WHO. *WHO Child Growth Standards: Methods and Development*. Available online at: <https://www.who.int/publications/i/item/924154693X>. WHO 2014 (accessed: Jun 6, 2021).
- WHO. *Executive Summary*. Available online at: <https://www.who.int/childgrowth/standards/velocity/tr3summary.pdf>. WHO 2014 (accessed: Jun 6, 2021).
- Argilés JM, López-Soriano FJ. The role of cytokines in cancer cachexia. *Med Res Rev*. (1999) 19:223–48. doi: 10.1002/(sici)1098-1128(199905)19:3<223::aid-med3>3.0.co;2-n
- Ladas EJ, Sacks N, Meacham L, Henry D, Enriquez L, Lowry G, et al. A multidisciplinary review of nutrition considerations in the pediatric oncology population: a perspective from children's oncology group. *Nutr Clin Pract*. (2005) 20:377–93. doi: 10.1177/0115426505020004377
- Sala A, Rossi E, Antillon F, Molina AL, de Maselli T, Bonilla M, et al. Nutritional status at diagnosis is related to clinical outcomes in children and adolescents with cancer: a perspective from Central America. *Eur J Cancer*. (2012) 48:243–52. doi: 10.1016/j.ejca.2011.06.006
- Ward EJ, Henry LM, Friend AJ, Wilkins S, Phillips RS. Nutritional support in children and young people with cancer undergoing chemotherapy. *Cochrane Database Syst Rev*. (2015) 2010:CD003298. doi: 10.1002/14651858.CD003298.pub3
- Jacquelin-Ravel N, Pichard C. Clinical nutrition body composition and oncology: a critical literature review of the synergies. *Crit Rev Oncol Hematol*. (2012) 84:37–46. doi: 10.1016/j.critrevonc.2012.02.001
- Pescatori LC, Savarino E, Mauri G, Silvestri E, Cariati M, Sardanelli F, et al. Quantification of visceral adipose tissue by computed tomography and magnetic resonance imaging: reproducibility and accuracy. *Radiol Bras*. (2019) 52:1–6. doi: 10.1590/0100-3984.2017.0211
- Jaimes C, Kirsch JE, Gee MS. Fast free-breathing and motion-minimized techniques for pediatric body magnetic resonance imaging. *Pediatr Radiol*. (2018) 48:1197–208. doi: 10.1007/s00247-018-4116-x
- Maddalo M, Zorza I, Zubani S, Nocivelli G, Calandra G, Soldini P, et al. Validation of a free software for unsupervised assessment of abdominal fat in MRI. *Phys Medica*. (2017) 37:24–31. doi: 10.1016/j.ejmp.2017.04.002
- Lee S, Kuk JL, Kim Y, Arslanian SA. Measurement site of visceral adipose tissue and prediction of metabolic syndrome in youth. *Pediatr Diabetes*. (2011) 12:250–7. doi: 10.1111/j.1399-5448.2010.00705.x
- O'Connor M, Ryan J, Foley S. Best single-slice location to measure visceral adipose tissue on paediatric CT scans and the relationship between anthropometric measurements, gender and VAT volume in children. *Br J Radiol*. (2015) 88:20140711. doi: 10.1259/bjr.20140711
- A collaborative statement from Dietitians of Canada, Canadian Paediatric Society, The College of Family Physicians of Canada, and Community Health Nurses of Canada. A health professional's guide for using the new WHO growth charts. *Paediatr Child Health*. (2010) 15:84–90. doi: 10.1093/pch/15.2.84
- Goodwin K, Syme C, Abrahamowicz M, Leonard GT, Richer L, Perron M, et al. Routine clinical measures of adiposity as predictors of visceral fat in adolescence: a population-based magnetic resonance imaging study. *PLoS ONE*. (2013) 8:e79896. doi: 10.1371/journal.pone.0079896
- WHO. *BMI-for-Age (5–19 Years)*. Available online at: <https://www.who.int/tools/growth-reference-data-for-5to19-years/indicators/bmi-for-age> (accessed: Jun 6, 2021).
- Kulaga Z, Litwin M, Tkaczyk M, Palczewska I, Zajackowska M, Zwolińska D, et al. Polish 2010 growth references for school-aged children and adolescents. *Eur J Pediatr*. (2011) 170:599–609. doi: 10.1007/s00431-010-1329-x

41. Barlow SE, Dietz WH. Obesity evaluation and treatment: expert committee recommendations. *Pediatrics*. (1998) 102:e29. doi: 10.1542/peds.102.3.e29

Conflict of Interest: The authors declare that the research was conducted in the absence of any commercial or financial relationships that could be construed as a potential conflict of interest.

Publisher's Note: All claims expressed in this article are solely those of the authors and do not necessarily represent those of their affiliated organizations, or those of the publisher, the editors and the reviewers. Any product that may be evaluated in

this article, or claim that may be made by its manufacturer, is not guaranteed or endorsed by the publisher.

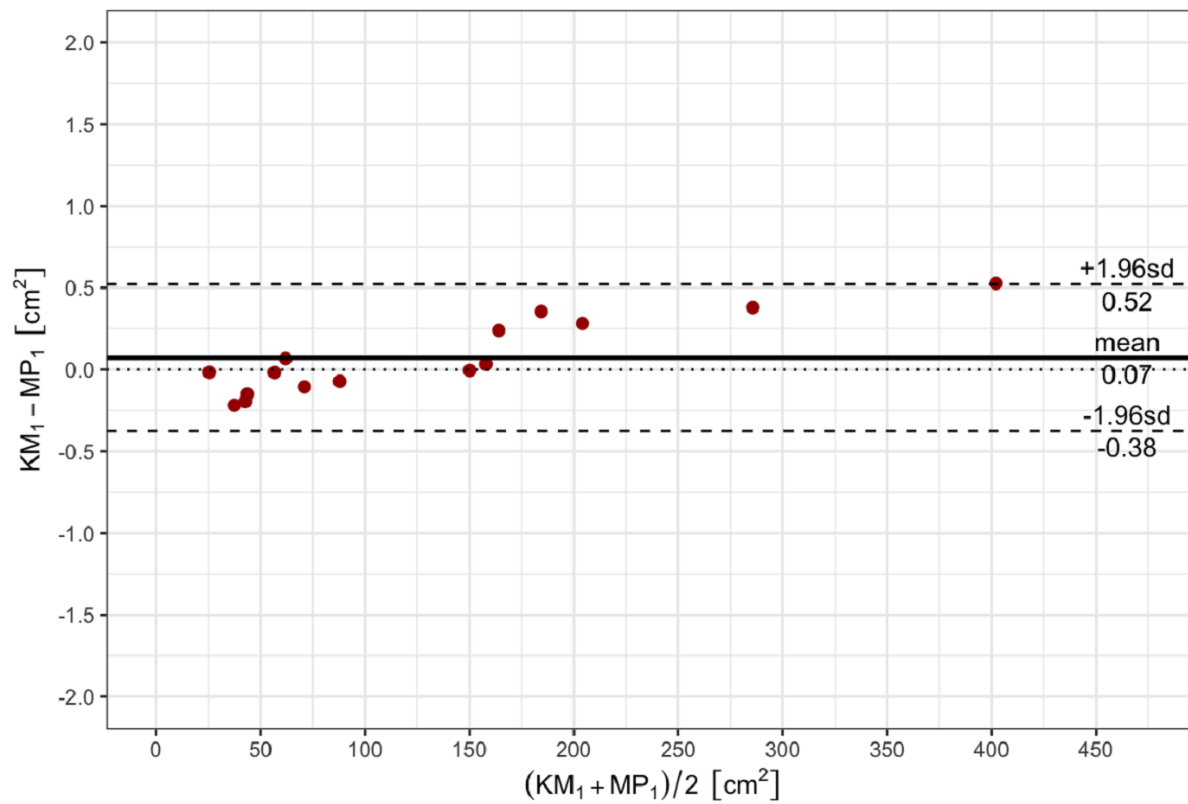
Copyright © 2021 Marunowski, Świętoń, Bzyl, Grzywińska, Kaszubowski, Bandosz, Khrichenko and Piskunowicz. This is an open-access article distributed under the terms of the Creative Commons Attribution License (CC BY). The use, distribution or reproduction in other forums is permitted, provided the original author(s) and the copyright owner(s) are credited and that the original publication in this journal is cited, in accordance with accepted academic practice. No use, distribution or reproduction is permitted which does not comply with these terms.

Supplementary Material

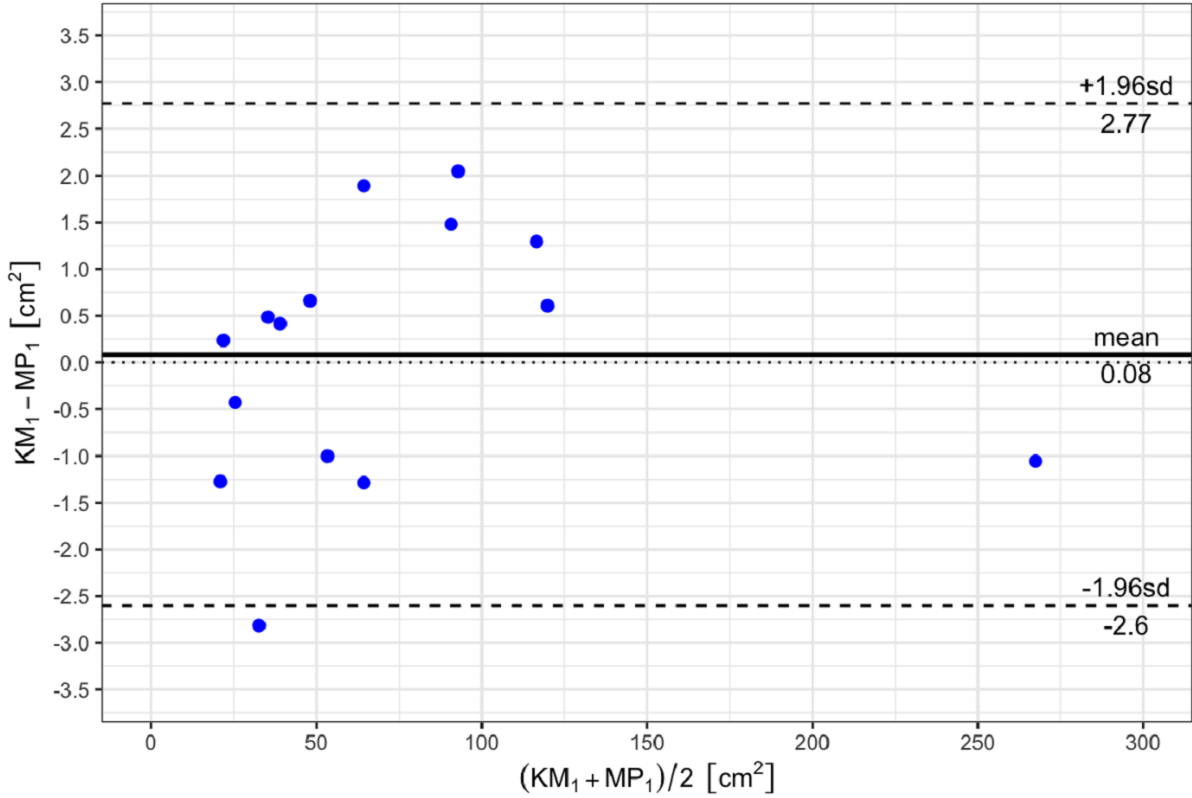
1 Supplementary Figures and Tables

1.1 Supplementary Figures

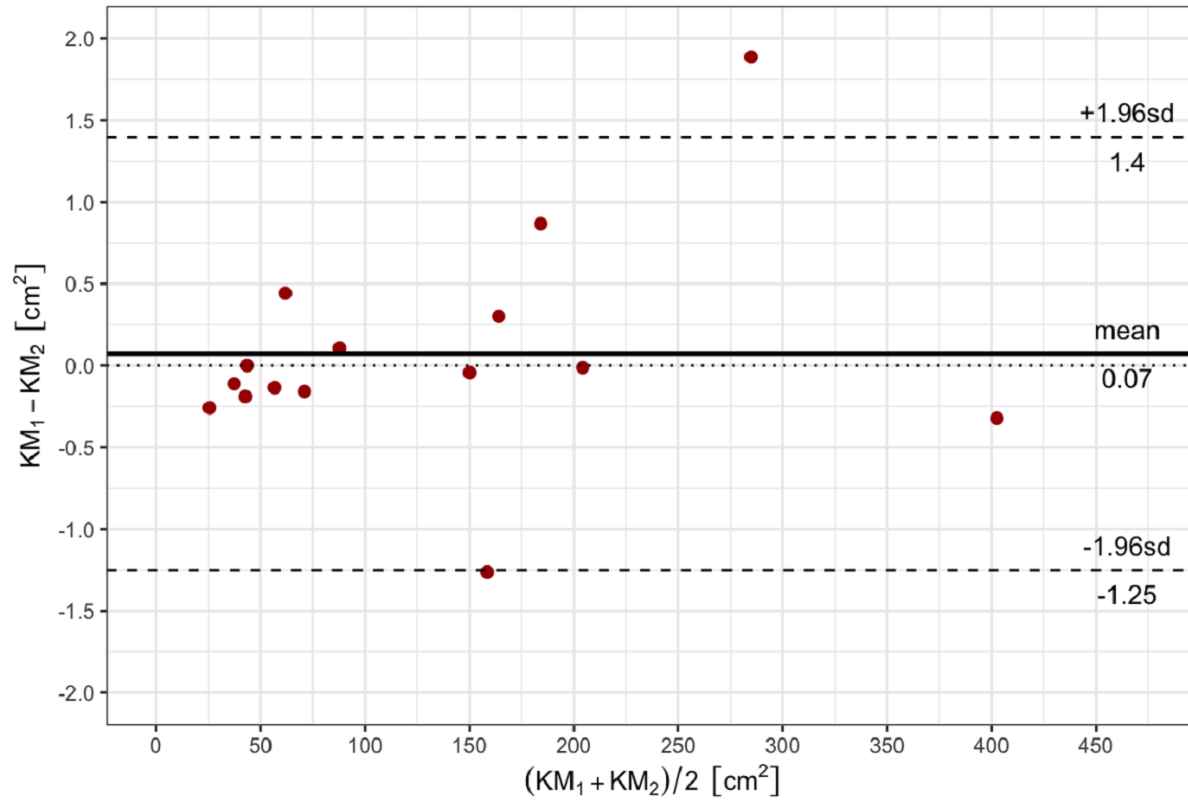
Supplementary Figure 1. Bland-Altman plot of the difference in interobserver SAT segmentation (cm^2) against the mean SAT segmentation (cm^2). KM, first radiologist; MP, second radiologist; SAT, subcutaneous adipose tissue; SD, standard deviation.



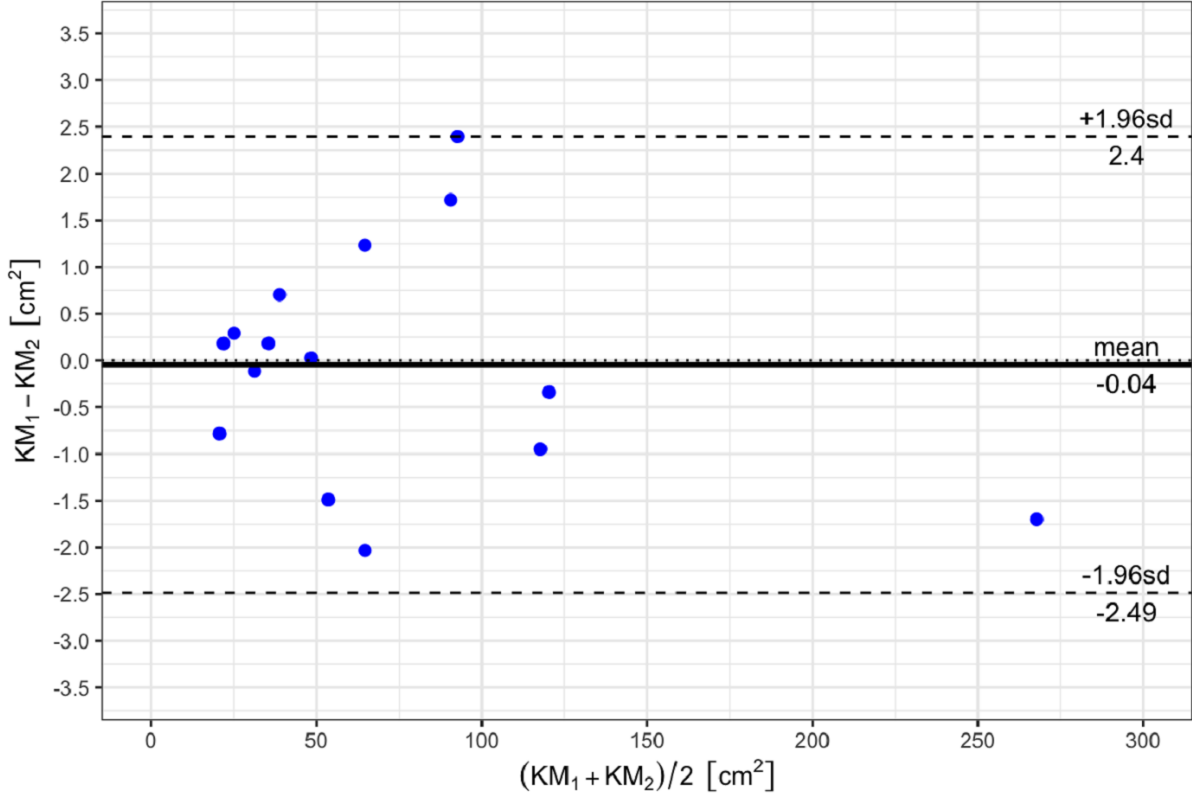
Supplementary Figure 2. Bland-Altman plot of the difference in interobserver VAT segmentation (cm^2) against the mean VAT segmentation (cm^2). KM, first radiologist; MP, second radiologist; SD, standard deviation; VAT, visceral adipose tissue.



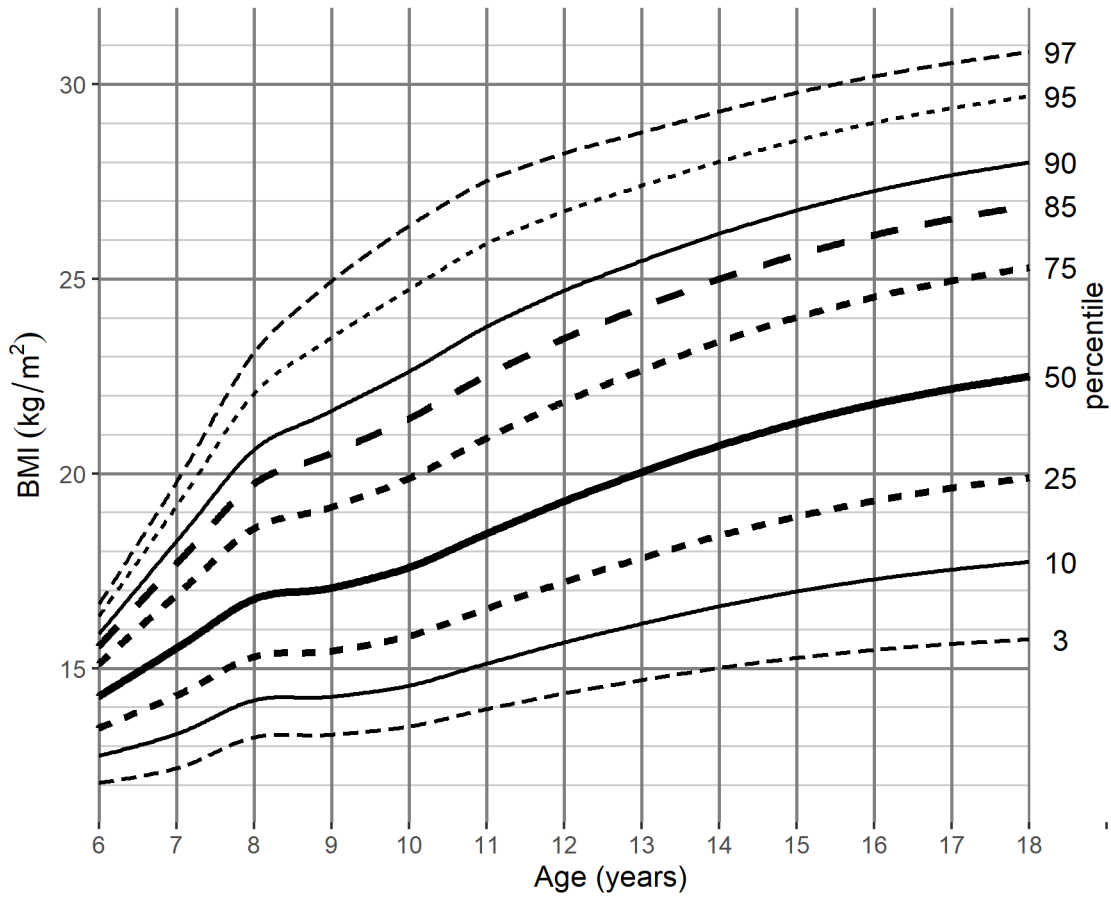
Supplementary Figure 3. Bland-Altman plot of the difference in intraobserver SAT segmentation (cm^2) against the mean SAT segmentation (cm^2). KM_1 , first radiologist, first measurement; KM_2 , first radiologist, second measurement; SAT, subcutaneous adipose tissue; SD, standard deviation.



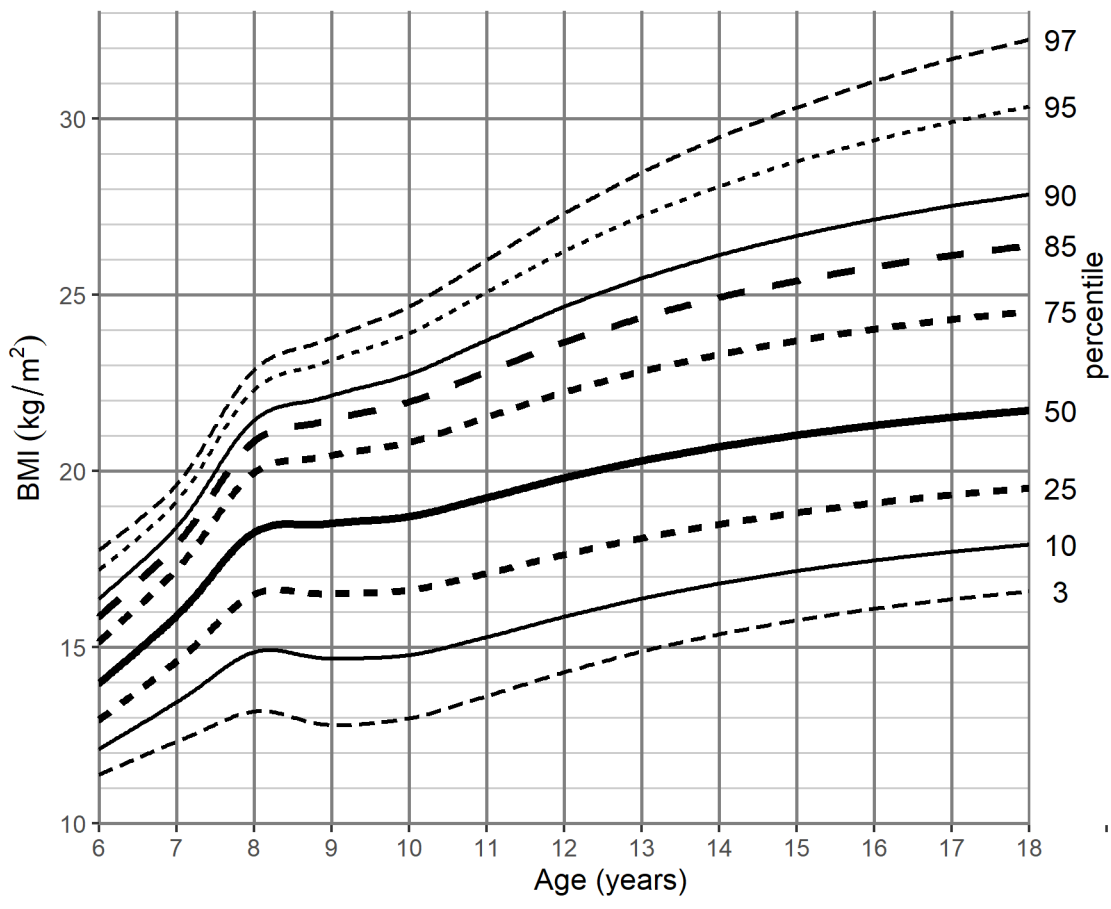
Supplementary Figure 4. Bland-Altman plot of the difference in intraobserver VAT segmentation (cm^2) against the mean VAT segmentation (cm^2). KM_1 , first radiologist, first measurement; KM_2 , first radiologist, second measurement; SD, standard deviation; VAT, visceral adipose tissue.



Supplementary Figure 5. BMI-for-age (kg/m^2) percentile charts for boys aged from 6 to 18 years. BMI, Body Mass Index.



Supplementary Figure 6. BMI-for-age (kg/m^2) percentile charts for girls aged from 6 to 18 years. BMI, Body Mass Index.



Reference values for MRI-derived psoas and paraspinal muscles and macroscopic fat infiltrations in paraspinal muscles in children

Kacper Marunowski¹ , Dominik Świętoń¹ , Włodzimierz Bzyl², Małgorzata Grzywińska³ , Piotr Bandosz⁴ , Dmitry Khrichenko⁵ & Maciej Piskunowicz^{1*} 

¹Department of Radiology, Medical University of Gdansk, Gdansk, Poland; ²Faculty of Mathematics, Physics, and Informatics, University of Gdansk, Gdansk, Poland; ³Department of Human Physiology, Medical University of Gdansk, Gdansk, Poland; ⁴Department of Prevention and Medical Education, Medical University of Gdansk, Gdansk, Poland; ⁵Division of Body Imaging, Department of Radiology, The Children's Hospital of Philadelphia, Philadelphia, PA, USA

Abstract

Background Sarcopenia, defined as loss of skeletal muscle mass, is a novel term associated with adverse outcomes in children. Magnetic Resonance Imaging (MRI) is a safe and precise technique for measuring tissue compartments and is commonly used in most routine paediatric imaging protocols. Currently, there is a lack of MRI-derived normative data which can help in determining the level of sarcopenia. This study aimed to introduce reference values of total psoas muscle area (tPMA), total paraspinal muscle area (tPSMA), and total macroscopic fat infiltrations of the PSMA (tMFI).

Methods In this retrospective study, the local database was searched for abdominal and pelvic region MRI studies of children aged from 1 to 18 years (mean age (standard deviation (SD)) of 9.8 (5.5) years) performed in the years 2010–2021. Children with chronic diseases and a history of surgical interventions were excluded from the analysis. Finally, a total of 465 healthy children ($n = 233$ girls, $n = 232$ boys) were enrolled in the study. The values of the tPMA, tPSMA, and tMFI were measured in square centimetres (cm^2) at the level of the L4/L5 intervertebral disc as the sum of the left and right regions. Age-specific and sex-specific muscle, fat, and body mass index percentile charts were constructed using the LMS method. Inter-observer agreement and intra-observer reproducibility were assessed using the Bland–Altman plots.

Results Both tPMA and tPSMA showed continuous increases in size (in cm^2) throughout all age groups. At the age of 18, the median tPMA areas reached 26.37 cm^2 in girls and 40.43 cm^2 in boys. Corresponding tPSMA values were higher, reaching the level of 40.76 cm^2 in girls and 56.66 cm^2 in boys. The mean value of tMFI within the paraspinal muscles was 5.0% (SD 3.65%) of their total area in girls and 3.5% (SD 2.25%) in boys with the actual difference between sexes up to 0.96 cm^2 . Excellent intra-observer reproducibility and inter-observer agreement were noted. Actual mean differences for tPMA were at the level of 0.43 and 0.39 cm^2 , respectively. Mean bias for tPSMA was 0.1 cm^2 for inter-observer and 0.05 cm^2 for intra-observer measurements.

Conclusions Our findings demonstrate novel and highly reproducible sex-specific MRI-derived reference values of tPMS, tPSMA, and tMFI at the level of the L4/L5 intervertebral disc for children from 1 to 18 years old, which may guide a clinician in the assessment of sarcopenia, a prognostic outcome marker in children.

Keywords Sarcopenia; Children; Normative values; Psoas and paraspinal muscles; Intramuscular fat

Received: 12 January 2022; Revised: 5 June 2022; Accepted: 13 June 2022

*Correspondence to: Maciej Piskunowicz, Department of Radiology, Medical University of Gdansk, Mariana Smoluchowskiego 17, 80-214 Gdansk, Poland. Tel: +48 58 349 36 80, Email: mpiskunowicz@wp.pl

Introduction

Malnutrition is a well-known phenomenon during the treatment of childhood cancer and multiple acute or chronic diseases.^{1–5} Loss of skeletal muscle mass and strength or exercise capacity (physical performance) in the adult population is called sarcopenia and has been described as a component of malnutrition. In the literature, paediatric sarcopenia is a new term associated with insufficient muscle mass at a given age and is an independent risk factor for surgical complications and neoplasm associated with severe adverse events.^{1,2,5–9}

There are many approaches for the initial assessment of muscle mass and nutritional status. The most readily available are anthropometric measures [body mass index (BMI), waist to height ratio (WtHR), mid-arm circumference, or skinfold thickness] as well as biochemical markers. Although anthropometric measurements are easy to use and less costly, they assess muscle mass indirectly with a high inter-observer variance which may limit sensitivity for detecting changes in these methods.^{10–13} A good correlation of muscle mass with biochemical markers has already been proven in a healthy population. However, their values may be imprecise due to disease-related complications such as organ failure or dietary factors.^{13,14}

The need for more precise measurements has resulted in the use of other methods such as bioelectrical impedance absorptiometry (BIA) and dual-energy X-ray absorptiometry (DXA). BIA is based on the assumption of the constant chemical composition of a fat-free-body.¹⁵ DXA uses two different energy spectra to differentiate bone and soft tissues based on tissue X-ray absorption.¹⁶ However, changes in body composition caused by disease-related complications such as ascites, organomegaly, organ failure, abnormalities in hydration status, or post-surgery changes limit their reproducibility in patients with chronic diseases.^{10,15,17}

Computed tomography (CT) overcomes these limitations by direct quantification of body compartments. The utility of CT in the assessment of sarcopenia based on a single slice at the abdominal level was already proven both in the adult and paediatric populations.^{2–4,6,8,18,19} Recently Eberhard *et al.* published normative values of psoas muscle area at the L3/L4 and L4/L5 intervertebral lumbar levels.²⁰ However, due to radiation exposure, the CT examination of abdominal and pelvic levels in children and adolescents is performed primarily during an emergency. Diagnostic and control tests of chronic diseases in these areas are performed using magnetic resonance imaging (MRI). MRI is a radiation-free technique and is considered the gold standard technique in soft tissues segmentation. It enables the assessment of muscle area as well as the measurement of intramuscular adipose tissue. As a measurement of cross-sectional muscle area at the L4/L5 intervertebral disc correlates with whole-body muscle mass and MRI is increasingly available in clinical centres, the evaluation of sarcopenic status can be included in the

routine diagnostic protocols of abdominal/pelvis cavity examinations.^{8,20,21} This study, therefore, was performed in a healthy paediatric population to establish the sex-dependent reference normative values of MRI-derived psoas and paraspinal muscles area and display a normal range of macroscopic fat infiltration into paraspinal muscles.

Material and methods

Patients

This retrospective, cross-sectional single-centre study was approved by the Institutional Ethics Committee (NKBBN/443/2018). The sample population included MRI examinations of the abdomen, pelvis, and lumbar spine in children and adolescents aged 0 to 18 years.

The dedicated search engine MedStream Designer (MSD) was used to search the local database for examinations performed in the years 2010–2021 where 2175 records were found. Exclusion criteria consisted of other body regions studies incorrectly found by MSD ($n = 433$), examinations without T2-weighted sequences in the transverse plane ($n = 27$), T2-weighted sequences distorted by artefacts ($n = 6$), children with a history of the oncological or haematological disease, ascites, glycogen storage diseases, muscular dystrophies, a chronic inflammatory/connective tissue diseases ($n = 637$), patients post nephrectomy or other surgical procedure ($n = 92$), children with severe scoliosis, bone or spinal canal disorders, and cerebral palsy ($n = 47$). Only the first MRI examination of changes with benign origin (e.g. liver haemangioma) was included while the rest of the follow-up studies were excluded from the analysis ($n = 104$). Initially found records included 364 examinations of children in the first year of life. Most of them were excluded due to malignancy and vesicoureteral reflux ($n = 328$), and only 16 records were considered healthy infants. Due to insufficient sample size, all data of children during infancy was excluded from further processing.

The final analysis included a total of 465 healthy children and adolescents aged 1 to 18 years ($n = 233$ girls, $n = 232$ boys). The patients' age, weight, and height at the time of MRI examination were obtained from DICOM header tags. Body mass index (BMI) was calculated for each subject by dividing weight in kilograms by the square of the height in meters. The differentiation of the study cohort by sex and age is available in the supplementary material (Supporting Information, Figure S8).

Imaging method

For evaluation of psoas muscle, paraspinal muscle, and paraspinal intramuscular fat areas, one slice at the level of

the L4/L5 intervertebral disc was chosen from the standard TSE T2-weighted sequence in the transverse plane. The images were obtained from different MRI systems: Philips Achieva 3.0 TX (Philips Medical Systems Netherlands, Best, the Netherlands) and two 1.5 T systems, Magnetom Aera and Magnetom Sola (Siemens Healthineers, Erlangen, Germany).

Muscle and fat tissue quantification

Images of all selected patients were retrieved from the local picture archiving and communication system. The first fully separated intervertebral space above the sacral bone was considered the L5/S1 level. On sagittal and coronal sequence images the L4/L5 intervertebral disc was identified and the corresponding axial image was selected. If the intervertebral disc was displayed on more than one cross-section, the image closer to the L4 vertebrae body was selected.

The muscle tissue was segmented into psoas (PMA) and paraspinal muscle (PSMA) compartments. The paraspinal compartment included multifidus, iliocostalis lumborum, and longissimus muscles. Both arms and other abdominal muscles were excluded from muscle tissue quantification. Macroscopic fat infiltrations into PSMA (MFI) were identified and excluded from final muscle areas.

Parametric Magnetic Resonance Imaging v1.2.31-b (pMRI) freeware available at the website www.parametricmri.com was used for semi-automatic body composition analysis.

The T2-weighted sequence was loaded into the volumetric region of interest (ROI) analysis module of pMRI software and processed for segmentation and volumetric quantification of selected tissues. Bilateral PMA and PSMA were delineated on corresponding axial cross-sectional images by the use of the free hand ROI mode. Signal intensity thresholds were manually set for the analysis of MFI. After corresponding free hand

and signal intensity-based segmentation, all data sets were visually revised and misclassified tissues were corrected.

The total PMA (tPMA), PSMA (tPMSA), and MFI (tMFI) represent the sum of the right and left ROIs (in cm²). Total muscle area (TMA) indicates the sum of tPMA and tPSMA muscles (in cm²).

Three hundred fifteen sets were segmented by K. M. (3rd year of specialization in radiology) and 150 sets by M. P. (radiologist with 15 years of experience in MRI). Additionally, the average time needed for analysis and correction of a single data set was approximately between 5 and 8 min. The example of the segmented cross-section is presented in *Figure 1A,B*.

Statistical analysis

Reproducibility of image segmentation

The inter-observer segmentation reproducibility between two independent radiologists (K. M. and M. P.) was assessed based on 40 sets of randomly selected MRI examinations. The evaluation of intra-observer reproducibility was conducted by re-segmentation (the time interval to first segmentation was at least 2 weeks) of the same set of images by one of the radiologists (K. M.) Based on these data, intra-observer and inter-observer agreement of the segmentation was assessed, using Bland–Altman plots with 95% agreement limits.²² Analysis was performed using R, version 4.1.0.

Statistical analysis of percentile charts

Sex-specific BMI-for-age, tPMA-for-age, tPSMA-for age, TMA-for-age and tMFI-for-age z-scores and percentile curves were analysed using the LMSChartMaker Light version 2.54 software.²³ The creation of growth centile standards was

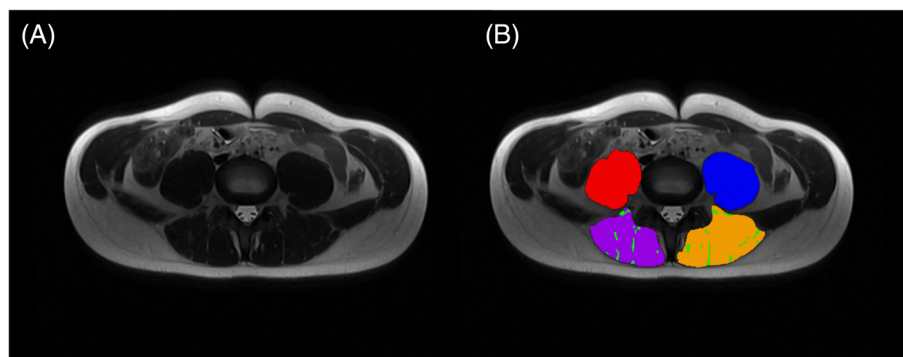


Figure 1 A 17-year-old boy (BMI: 19.4 kg/m²). (A) Native MRI T2-weighted sequences in the transverse plane at the level of L4/L5 intervertebral disc. (B) Example of tissue segmentation at the same level: Right PMA (red), left PMA (blue), right PSMA (purple), left PSMA (yellow) and tMFI (green). BMI, body mass index; PMA, psoas muscle area; PSMA, paraspinal muscle area; tMFI, total macroscopic fat infiltrations into PSMA.

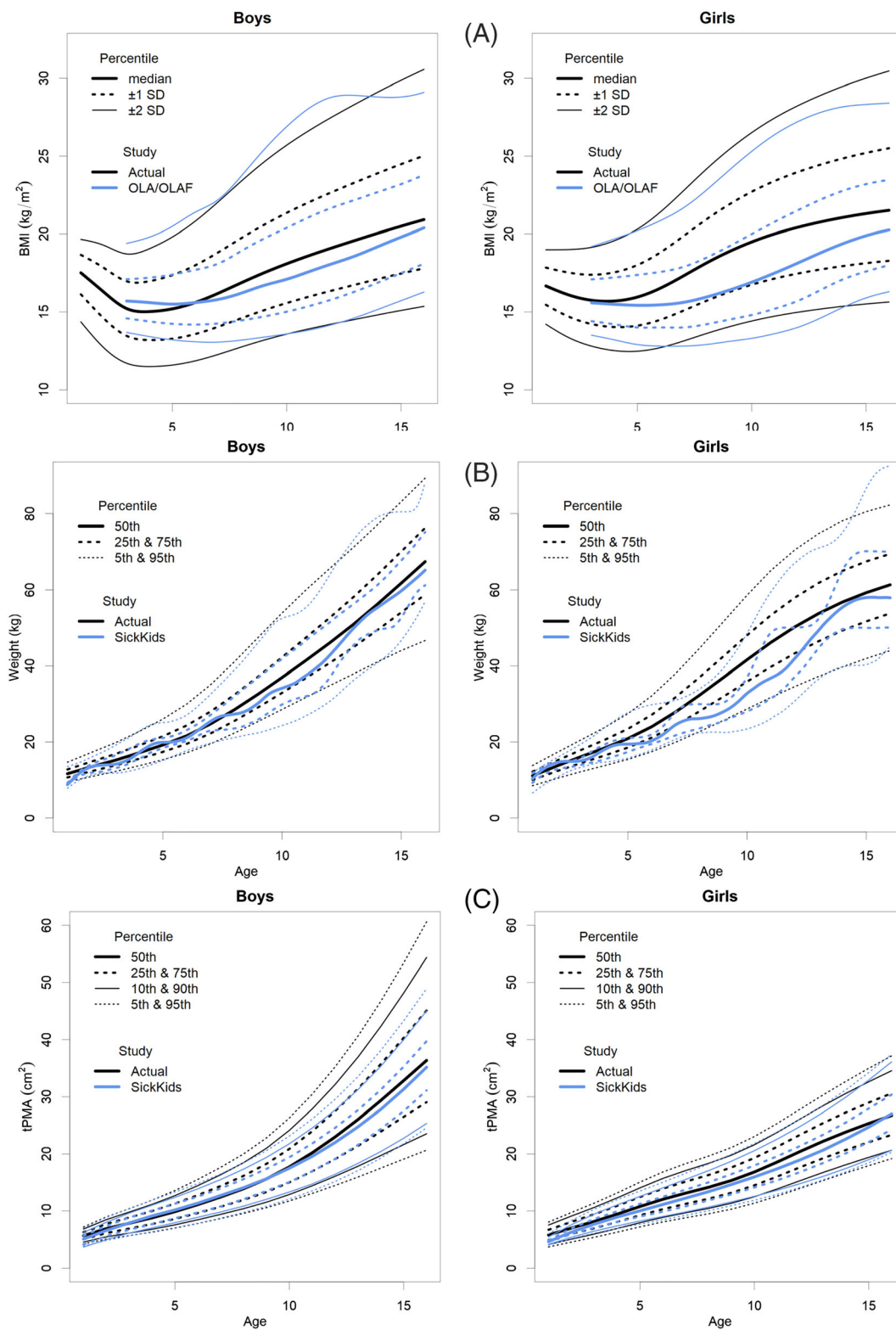


Figure 2 (A) BMI-for-age (kg/m²) SD percentile charts for boys and girls aged from 1 to 16 years of actual study in comparison with national reference standards (OLA/OLAF study).^{26,27} BMI, body mass index; SD, standard deviation. (B) Weight-for-age (kg) percentile charts for boys and girls aged from 1 to 16 years in comparison with weight reference standards published by Eberhard *et al.*¹⁷ (C) MRI-derived total-psoas-for-age (cm²) percentile charts for boys and girls aged from 1 to 16 years in comparison with tPMA CT-derived reference standards published by Eberhard *et al.*¹⁷ tPMA, total psoas muscle area.

based on the lambda-mu-sigma method.²⁴ The LMS parameters consist of the median (M), the generalized coefficient of variation (S), and the power in the Box-Cox transformation (L). By the use of Box-Cox, power transformation measurement for any given age can be brought closest to normality, where age is used as a continuous variable. In the preparation stage, the z-score plot of each variable was inspected for the identification of outliers. None of the outliers were considered to be made due to mistakes in data recording or transferring.

Following WHO guidelines,²⁵ derivation of percentiles was enabled only within the interval of z-scores between -3.0 and 3.0 . To prevent distortions of percentile charts due to outliers, the data beyond the limits of observed values were fixed at the distance of -2.5 standard deviation (SD) and 2.5 SD at each age correspondingly. Both in boys and girls only two BMI values were fixed. All muscles and tMFI values were within the range of set limits.

The age-dependent variation of three smooth curves representing $L(t)$, $M(t)$, and $S(t)$ were created from the original data by fitting natural cubic splines with knots at each distinct age t :

$$C\alpha(t) = M(t) \times [1 + L(t) \times S(t) \times Z\alpha]^{1/L(t)}$$

where $Z\alpha$ is the α -quantile of a standard normal distribution and $C\alpha(t)$ is a percentile corresponding to $Z\alpha$. Equivalent degrees of freedom (edf) $L(t)$, $M(t)$, and $S(t)$ measure the complexity of each fitted curve. In our data set, each model was fitted with the loop option. As further fitting made no significant improvements to our models, the standard edf of L3, M5, and S3 was chosen.²³

Results

The image segmentation reproducibility analysis showed good agreement for the measurements at the L4/L5 intervertebral level. For tPMA, the mean intra-observer and inter-observer disagreements were at the level of 0.43 and 0.39 cm^2 , respectively. On the Bland–Altman intrarater plot, 4 outliers can be spotted, however, most measurements varied up to 1.2 cm^2 . Between independent radiologists, almost all of the actual differences were within the range of 1 cm^2 . The variation and maximal differences of tPSMA actual measurements were slightly higher than tPMA reaching 2 cm^2 for inter-observer and to 1.75 cm^2 for the intra-observer difference. However, the bias of mean differences was lower with corresponding values of 0.1 and 0.05 cm^2 . The mean tMFI intra-observer and inter-observer differences were at levels of 0.77 and 0.91 cm^2 , respectively. On the Bland–Altman plots, a few outliers can be spotted; however, most actual disagreements were within the range of 1.2 cm^2 for intra-observer and 1.9 cm^2 for inter-observer measurements. The differences between observers in the form of Bland–Altman plots are available in the supplementary material (Figures S1–S6).

The BMI-for-age, tPMA-for-age, tPSMA-for-age, TMA-for-age, and tMFI-for-age percentile charts were constructed based on the 465 MRI examinations of children (233 girls and 232 boys) aged 1 to 18 years (mean age (SD) of 9.8 (5.5) years). For male subjects mean age (SD) was 9.46 (5.31) years. For female subjects mean age (SD) was 10.11 (5.68) years.

The current charts of BMI increase in correlation with age, including SD curves (-2SD , -1SD , median, $+1\text{SD}$, $+2\text{SD}$) and a

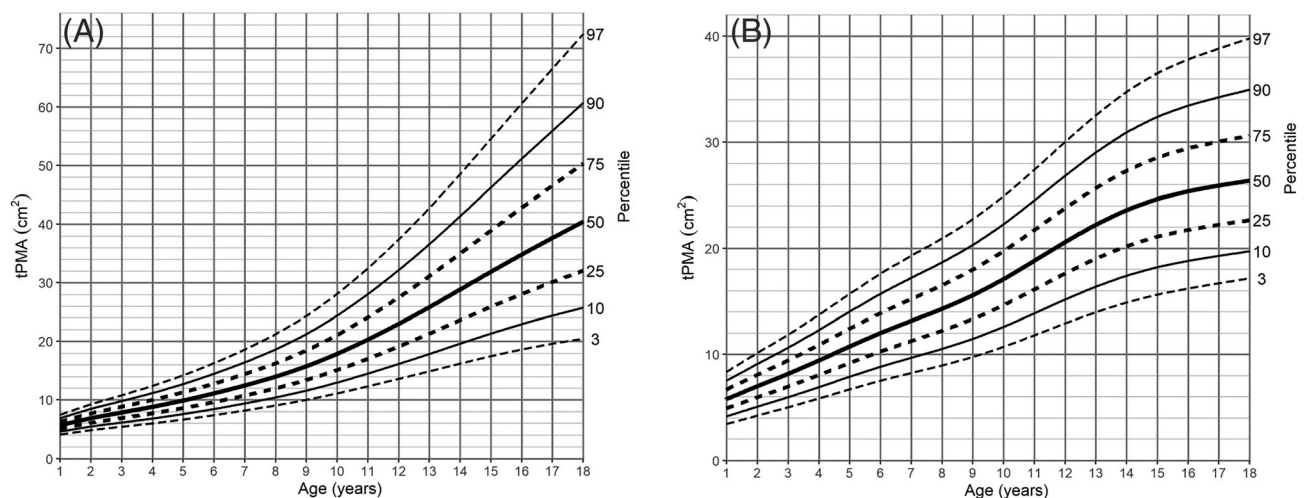


Figure 3 Psoas-for-age (cm^2) percentile charts for (A) boys and (B) girls aged from 1 to 18 years. tPMA, total psoas muscle area.

comparison with the largest BMI study of the Polish population, “Ola/Olaf” are shown in *Figure 2A*.^{26,27} The present study found that the BMI z-scores were higher compared with the national Ola/Olaf reference values, especially in the range of +2 SD and +1 SD, where the differences reached 2.7 units in girls and 1.46 units in boys. As the study population of currently available CT-derived norms for total psoas muscle area is defined by weight,²⁰ the comparison of weights with our results is presented in *Figure 2B*.

The tPMA and tPSMA reference values for boys and girls in each age group are presented in *Tables S1* and *S2*. Corresponding data for TMA is included in *Table S3*. Based on the results, percentile charts were created for each muscle compartment (*Figures 3A,B, 4A,B, and S7A,B*). In all age groups, there was a continuous increase in both tPMA and tPSMA. The sex percentiles values were similar in the first 8 years of life for tPMA and the first 10 years of life for tPSMA, with a later predominance of boys in the following years. In girls, the most dynamic increase in tPMA area was recorded between the ages of 9 and 14, reaching a median of 26.37 cm² at the age of 18. In boys, a dynamic increase of tPMA was observed until the end of the observed range. At this age, a median of 40.43 cm² was reached. The sex distribution of tPSMA percentiles was different in children 14 years of age and older. In boys, an increase was noted within all age groups, while in girls, stability was reached around the age of 15 years. The medians of tPSMA surface at the end of the observed age reached values of 56.66 and 40.76 cm², respectively.

No substantial differences between sexes were noted in the surface area of tMFI from age 1 to 3 years old. In older children, female predominance was observed, especially prominent during adolescence (for medians, the difference of 0.34–0.96 cm²). The mean value of tMFI reached up to 5% (SD 3.65%) in girls and 3.5% (SD 2.25%) in boys. The distribu-

tion of percentile charts in our population showed a continuous increase observed across all age groups with a steep increase in girls from the age of 8 years onwards (*Table S4, Figure 5A,B*).

Discussion

This study proposed sex-specific MRI-derived reference values as percentile charts of the psoas muscle, paraspinal muscles, and macroscopic fat infiltrations in paraspinal muscles areas for children aged from 1 to 18 years. This is the first study that demonstrates normative values of paraspinal muscle and macroscopic fat infiltrations in paraspinal muscles included in the whole single-slice muscle area. Until now, intramuscular fat of children’s paraspinal muscles was only described as circular ROI fat fraction.²⁸

With skeletal muscle mass increasing during growth, many pathological states such as malignancies, post-surgery, or inflammatory diseases may lead to inadequate muscle mass for a given age.^{1,2,14} This state, called sarcopenia, is associated with adverse health outcomes during treatment and a decrease of life quality, mainly described in the adult population.^{14,18,19,29} However, this phenomenon has been described more and more recently in paediatric populations.^{2,5–7,9}

Currently available methods of measuring sarcopenia are often implicated in disease-related conditions and appear to be inadequate to meet the demands of personalized medicine that is easily incorporated into clinical practice.³⁰

Radiological direct measurements of cross-sectional muscle area at the lumbar level are proven objective and feasible methods to assess sarcopenia.^{3,5,6} In a recently published

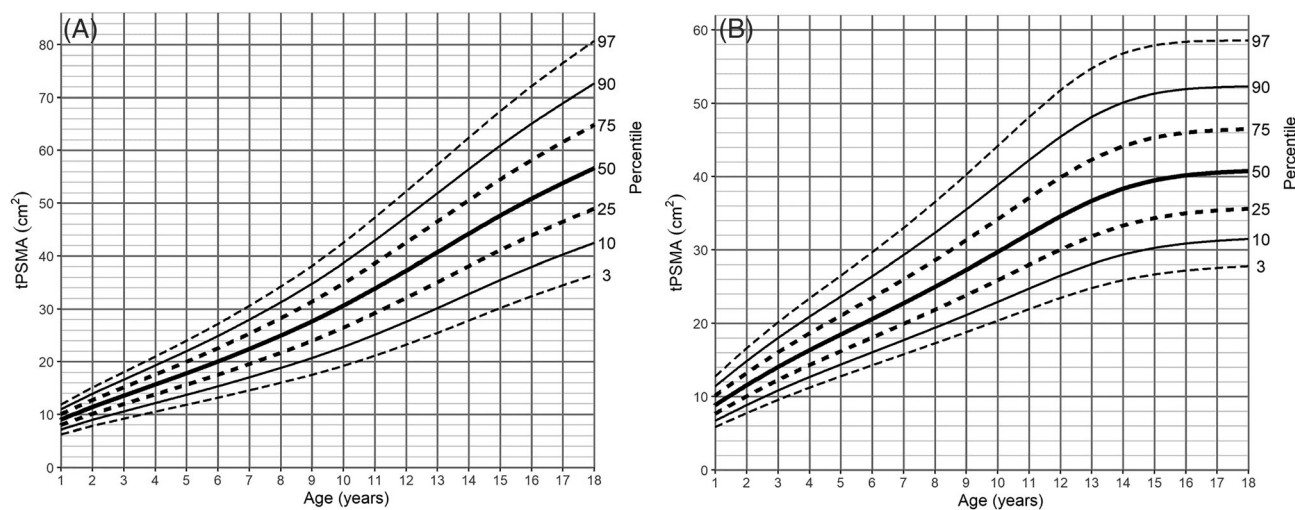


Figure 4 Paraspinal muscle-for-age (cm²) percentile charts for (A) boys and (B) girls aged from 1 to 18 years. tPSMA, total paraspinal muscle area.

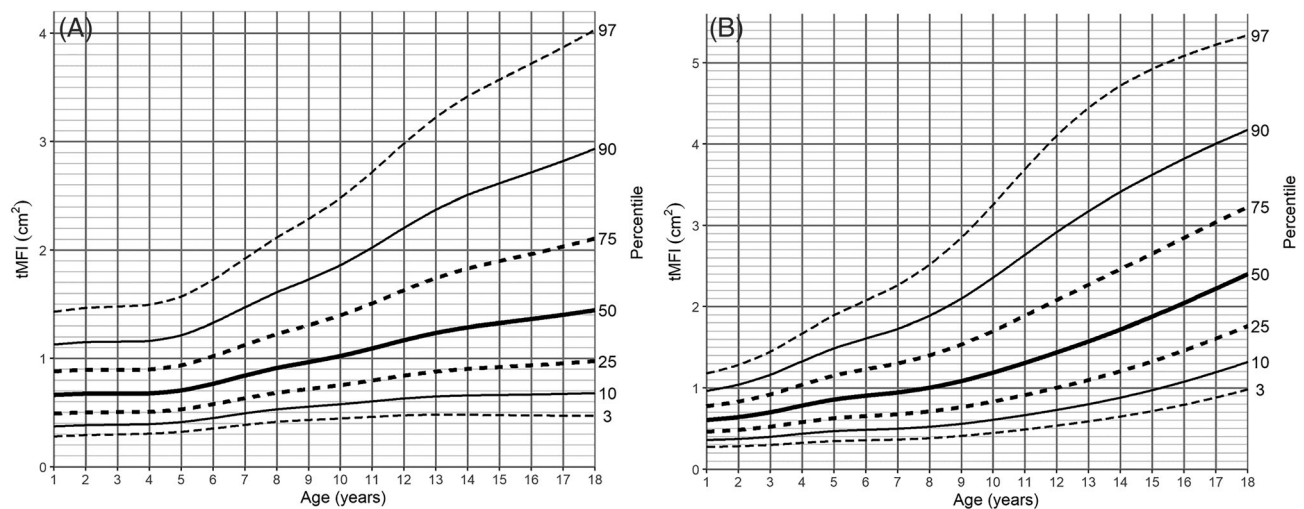


Figure 5 tMFI-for-age (cm^2) percentile charts for (A) boys and (B) girls aged from 1 to 18 years. tMFI, total macroscopic fat infiltrations in paraspinal muscles.

study, the reference values for total psoas muscle area were established in a group of children 1–16 years old who required emergency abdominal CT examination after paediatric trauma.²⁰ However, most malnutrition abnormalities leading to sarcopenia are diagnosed with MRI. Unlike CT, this imaging method is a preferred part of many paediatric diagnostic protocols, free from ionizing radiation, with much better ‘soft tissue contrast’ than CT.

The reproducibility of MRI examination of tPMA was already demonstrated in the literature.^{5,31} Excellent intra-observer and inter-observer agreements were observed in our study (*Figures S1–S4*). The mean disagreement of tPMA surface area at the level of the L4/L5 intervertebral disc obtained by the use of a semi-automatic method was higher than tPSMA by 0.33 cm^2 in intra-observer and by 0.34 cm^2 in the inter-observer group. However, actual maximal differences were higher in the group of paraspinal muscles. It indicates a greater variety of measurements with a similar spread on both sides of the middle line. In both muscle groups, the reader (M. P.) selected slightly larger muscle areas than the second reader (K. M.), but the difference was insignificant. The high inter-observer agreement obtained in our study indicates the feasibility of tissue area percentile charts based on our results.

Accurate and reproducible measurement of adipose and muscle areas based on MRI examinations requires the involvement of personnel experienced with this method. The assessment of full muscle length is time-consuming and often impossible due to the limitation of the area included in the examination. Moreover, adding dedicated sequences to fully appreciate selected muscles will increase the time of examination and cost, as well as sedation time in younger children.

Following previous studies, estimation of muscle mass based on a single cross-section is highly accurate; therefore,

such an approach is currently the most cost and time-efficient option.^{21,29,32,33} In the paediatric population, the utility of manual measurement was already proven for tPMA and tPSMA.^{2–4,6} Additionally, previous studies noted a continuous increase of both tPMA and tPSMA during the first 20 years of life.³⁴ In comparison, accurate quantification of smaller muscles (e.g. abdominal oblique muscles) is possible only when bordering tissues have different signal intensity such as fat. The abdominal wall in the youngest and thinnest children contains little adipose tissue, which limits the proper identification of muscle margins.

In the published articles, few paediatric measurement sites were proposed, with the level of the third lumbar vertebrae being most frequently used.^{1,2,5,6,8} Recent studies introduced the level of the L4/L5 intervertebral disc as a feasible cross-section for single-slice measurements in children.^{3,20} Lurz *et al.*²⁰ proved the interchangeability of L3/L4 and L4/L5 intervertebral disc levels for tPMA measurement in both sexes ($r = 0.95–0.98$, $P < 0.001–0.01$). According to authors, the tPMA differs depending on the measured level with the largest area noted at the level of the upper L5 vertebrae endplate. In comparison, the largest tPSMA was reported at the level of the upper L3 vertebrae endplate, whereas the area was slightly smaller at levels of L4 and L5 vertebrae, but not significant.³⁴ In clinical settings, paediatric MRI examination of both pelvis and abdominal region usually covers the L4/L5 level which allows utilization of percentile charts in a greater variety of pathological conditions. Therefore, we had chosen this region as a reference level in our study.

The results of BMI SD scores for children from 1 to 4 years old present a similar configuration to WHO normative values.^{25,35} The distribution of BMI percentile lines of older children in comparison with national Ola/Olaf BMI standards was similar, however, our results for the majority of the time

were higher^{26,27} (Figure 2A). This was particularly observed for girls from the fifth year of life onwards. The disagreement may be related to our patient study population which included only the Caucasian race. On the other hand, an increase in mean weight and BMI was reported over the years.³⁶ The WHO and Ola/Olaf BMI data represent standards from before the year 2010 which may create a slight bias in comparison with the current weight distribution. Bodyweight percentile lines also showed a noticeable difference compared with the Canadian study, while the children included in our study were heavier²⁰ (Figure 2B).

A further interesting observation in our study is a noticeable difference between sexes for both tPMA and tPSMA percentile lines. In the early years of life, the differences in muscle areas between boys and girls are small; however, from the age of 8 for tPMA and the age of 10 for tPSMA, a greater difference can be noticed in boys. At the end of observed age, flattening of both muscle percentile curves in girls is noticeable, which may be associated with an earlier end of growth phase than in boys. At the end of the observed age range, the slope of percentile lines of tPMA in our study is similar to previously published norms in CT²⁰ (Figure 2C). When compared with the Canadian study,²⁰ our 75th, 90th, and 95th tPMA percentile lines tend to have a little bit greater differences in older children. It may be the result of an insufficient sample size and also a greater variance of results of enrolled children. However, considering the difference in populations, tPMA growth tendencies between both studies showed high convergence overall.

Measurement of muscle area in the paediatric population was already conducted by the use of both T1-weighted and T2-weighted sequences,^{5,31} while MFI was only evaluated in T1-weighted water-fat sequences (called Dixon sequence).²⁸ T1-weighted Dixon sequence is characterized by short acquisition time, however, is vulnerable to movement and breathing artefacts, which occur much more often in children than adults especially if children are sedated. Hence, for MFI evaluation, we decided to use regular T2-weighted sequences which are part of standard abdominal and pelvis examination and their sensitivity and specificity in the assessment of adipose tissue are comparable with T1-weighted sequences.³⁷ During adolescence and early adulthood, greater quantities of intramuscular fat were observed in girls than boys, which is compatible with higher fat content in females. The mean value of tMFI in our study (3.5% in boys and 5% in girls) is consistent with available data.³⁸ As body fat fraction increases during chronic diseases, malignancies, and treatment with specific drugs (e.g. steroids),³⁹ area-for-age normative values may be used to estimate the degree of fat infiltration. In those cases, it is especially important to measure fat-free muscle area as the inclusion of MFI may delay the diagnosis of sarcopenia. Additionally, it was reported that the functionality of lower extremity muscles seems to be disturbed by fat infiltrations.⁴⁰ We suspect that similar changes occur in

paraspinal muscles, which alongside muscle loss in sarcopenia may further decrease physical performance. It indicates that the assessment of MFI may become part of the initial evaluation during hospitalization in the future.

This study also has several limitations. Firstly, our study was performed at a single institution; therefore, our results only refer to the Caucasian population. Secondly, there is a lack of percentile charts for children in the first year of life. It was caused by an insufficient number of healthy participants because most MRI examinations of the abdomen and pelvis were performed for oncological reasons. Further, the tPMA, tPSMA, and tMFI were not standardized by height, which limits the consistency of measurements across the range of growing deficits. However, height in children depends on both constitutional and health-related variables. Growth deficits and sarcopenia are often related to the same underlying conditions. Height-standardization, may improve the performance of charts but also introduce overcorrection, especially in long-lasting diseases which are affecting the subject's height. Currently, there is a lack of MRI-derived reference values in the paediatric population, and in CT-based percentile charts height correction was not performed.²⁰ Additionally, the distribution of BMI charts in our group was similar to the national growth charts which reflect the general population of Poland^{26,27} (Figure 2A). Therefore, no correction for height was performed, and we accepted the methodology consistent with previous studies.²⁰ Instead, we rather recommend the clinical use of percentile charts taking into account the broader clinical context. The last limitation includes the inability to estimate confidence intervals for each percentile line during the construction of charts and the time necessary to perform semi-automatic segmentation of tissues. Multicentre studies on larger populations may require the implementation of fully automatic tools such as currently rapidly developing deep learning algorithms.

In conclusion, our study is the first to define MRI-derived reference values of tPMA and tPSMA in the form of percentile charts for children aged from 1 to 18 years. Additionally, tMFI was measured and first age-dependent norms for boys and girls during childhood and adolescence were presented. In the view of personalized medicine, early detection of sarcopenia and macroscopic fat infiltrations into paraspinal muscles seems to be one of the important directions in paediatric medicine. Incorporation of our method into standard diagnostic protocols may enable a precise initial assessment of sarcopenic status and appropriate nutritional support.

Conflict of interest

Kacper Marunowski, Dominik Świętoń, Włodzimierz Bzyl, Małgorzata Grzywińska, Piotr Bandosz, Dmitry Khrichenko, and Maciej Piskunowicz declare that they have no conflict of interest.

Funding

This study received no specific grant from any funding agency in the public, commercial, or not-for-profit sectors.

Online supplementary material

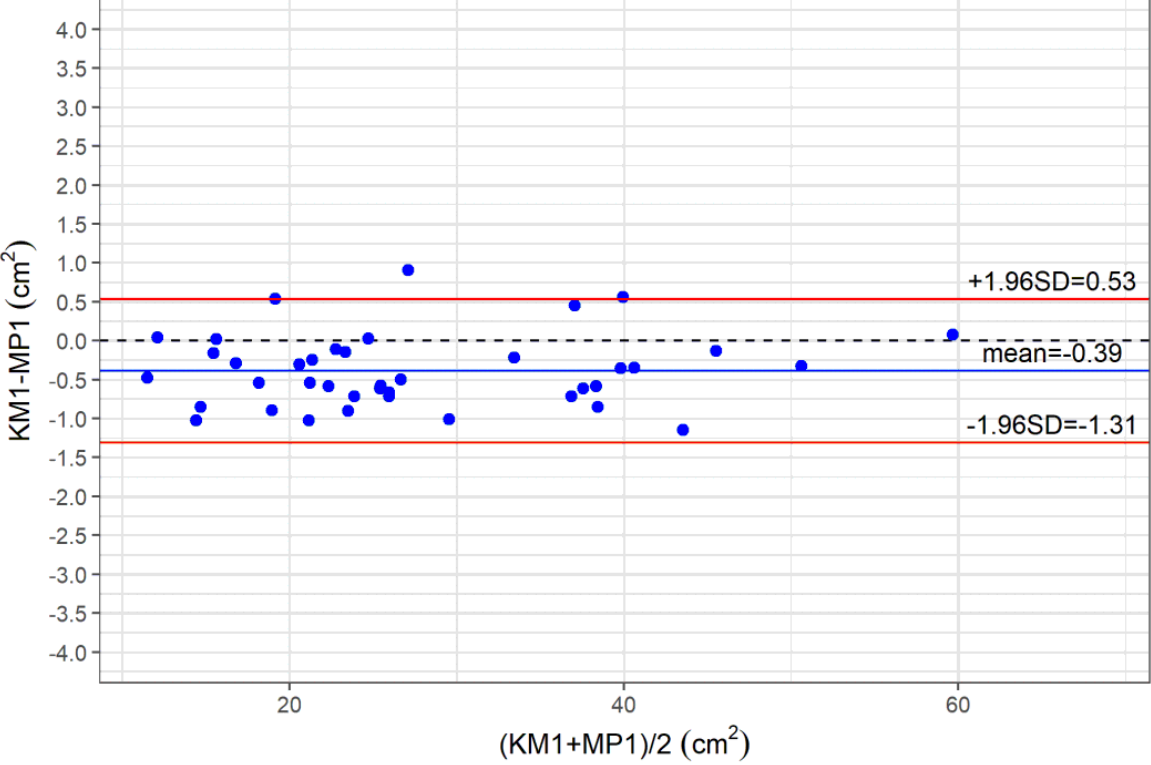
Additional supporting information may be found online in the Supporting Information section at the end of the article.

References

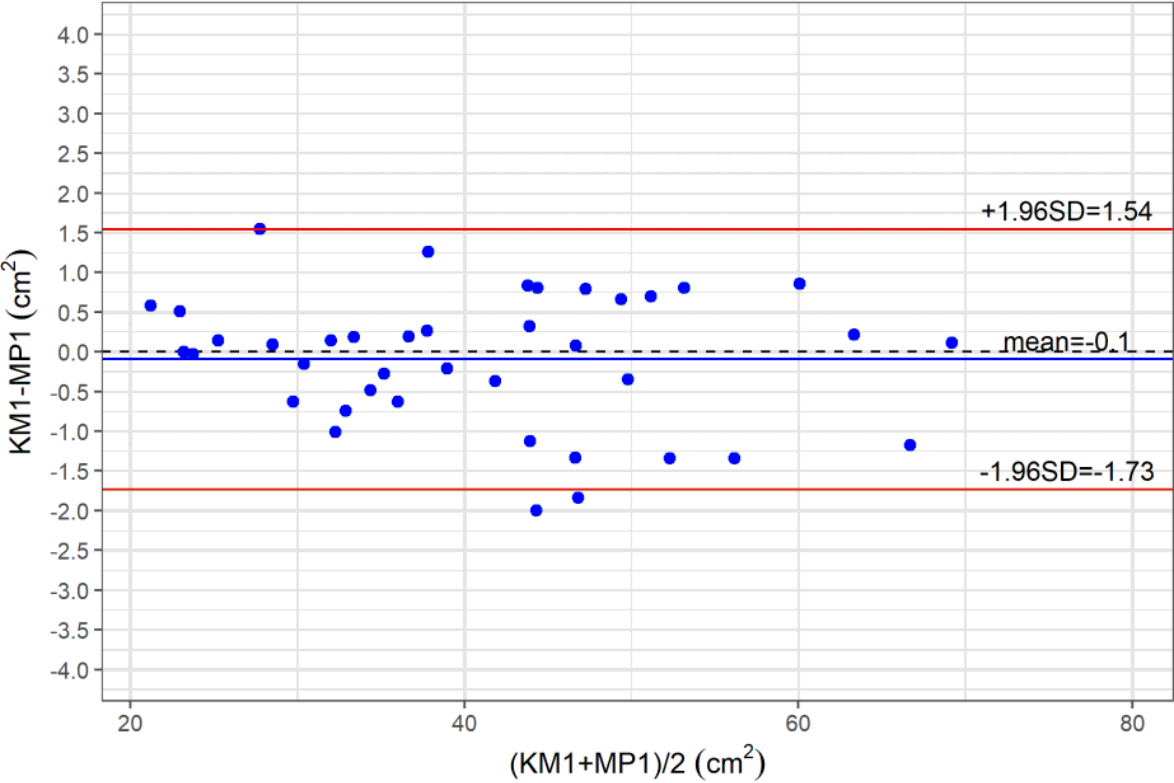
- Suzuki D, Kobayashi R, Sano H, Hori D, Kobayashi K. Sarcopenia after induction therapy in childhood acute lymphoblastic leukemia: its clinical significance. *Int J Hematol* 2018;**107**:486–489.
- López JJ, Cooper JN, Albert B, Adler B, King D, Minneci PC. Sarcopenia in children with perforated appendicitis. *J Surg Res* 2017;**220**:1–5.
- Lurz E, Patel H, Frimpong RG, Ricciuto A, Kehar M, Wales PW, et al. Sarcopenia in Children With End-Stage Liver Disease. *J Pediatr Gastroenterol Nutr* 2018;**66**:222–226.
- Mangus RS, Bush WJ, Miller C, Kubal CA. Severe Sarcopenia and Increased Fat Stores in Pediatric Patients With Liver, Kidney, or Intestine Failure. *J Pediatr Gastroenterol Nutr* 2017;**65**:579–583.
- Dedhia PH, White Y, Dillman JR, Adler J, Jarboe MD, Teitelbaum DH, et al. Reduced paraspinal muscle area is associated with post-colectomy complications in children with ulcerative colitis. *J Pediatr Surg* 2018;**53**:477–482.
- Kawakubo N, Kinoshita Y, Souzaki R, Koga Y, Oba U, Ohga S, et al. The Influence of Sarcopenia on High-Risk Neuroblastoma. *J Surg Res* 2019;**236**:101–105.
- Rayar M, Webber CE, Nayiager T, Sala A, Barr RD. Sarcopenia in Children With Acute Lymphoblastic Leukemia. *J Pediatr Hematol Oncol* 2013;**35**:98–102.
- Ooi PH, Thompson-Hodgetts S, Pritchard-Wiart L, Gilmour SM, Mager DR. Pediatric Sarcopenia: A Paradigm in the Overall Definition of Malnutrition in Children? *J Parenter Enteral Nutr* 2020;**44**:407–418.
- Ritz A, Froeba-Pohl A, Kolorz J, Vigodski V, Hubertus J, Ley-Zaporozhan J, et al. Total Psoas Muscle Area as a Marker for Sarcopenia Is Related to Outcome in Children With Neuroblastoma. *Front Surg* 2021;**8**:718184.
- Horan M, Gibney E, Molloy E, McAuliffe F. Methodologies to assess paediatric adiposity. *Irish J Med Sci (1971)* 2015;**184**:53–68.
- Blijdorp K, van den Heuvel-Eibrink MM, Pieters R, Boot AM, Delhanty PJD, van der Lely A-J, et al. Obesity Is Underestimated Using Body Mass Index and Waist-Hip Ratio in Long-Term Adult Survivors of Childhood Cancer. *PLoS ONE* 2012;**7**:e43269.
- Orgel E, Mueske NM, Spoto R, Gilsanz V, Freyer DR, Mittelman SD. Limitations of body mass index to assess body composition due to sarcopenic obesity during leukemia therapy. *Leuk Lymphoma* 2018;**59**:138–145.
- Rubbieri G, Mossello E, Di Bari M. Techniques for the diagnosis of sarcopenia. *Clin Cases Miner Bone Metab* 2014;**11**:181–184.
- Ryan E, McNicholas D, Creavin B, Kelly ME, Walsh T, Beddy D. Sarcopenia and Inflammatory Bowel Disease: A Systematic Review. *Inflamm Bowel Dis* 2019;**25**:67–73.
- Sizoo D, de Heide LJM, Emous M, van Zutphen T, Navis G, van Beek AP. Measuring Muscle Mass and Strength in Obesity: a Review of Various Methods. *Obes Surg* 2021;**31**:384–393.
- Pietrobelli A, Formica C, Wang Z, Heymsfield SB. Dual-energy X-ray absorptiometry body composition model: review of physical concepts. *Am J Physiol Metab* 1996;**271**:E941–E951.
- Buckinx F, Landi F, Cesari M, Fielding RA, Visser M, Engelke K, et al. Pitfalls in the measurement of muscle mass: a need for a reference standard. *J Cachexia Sarcopenia Muscle* 2018;**9**:269–278.
- Amini B, Boyle SP, Boutin RD, Lenchik L. Approaches to Assessment of Muscle Mass and Myosteatosis on Computed Tomography: A Systematic Review. *J Gerontol Ser A* 2019;**74**:1671–1678.
- Jones KI, Doleman B, Scott S, Lund JN, Williams JP. Simple psoas cross-sectional area measurement is a quick and easy method to assess sarcopenia and predicts major surgical complications. *Colorectal Dis* 2015;**17**:O20–O26.
- Lurz E, Patel H, Lebovic G, Quammie C, Woolfson JP, Perez M, et al. Paediatric reference values for total psoas muscle area. *J Cachexia Sarcopenia Muscle* 2020;**11**:405–414.
- Lacoste Jeanson A, Dupej J, Villa C, Brůžek J. Body composition estimation from selected slices: equations computed from a new semi-automatic thresholding method developed on whole-body CT scans. *PeerJ* 2017;**5**:e3302.
- Bland JM, Altman DG. Measuring agreement in method comparison studies. *Stat Methods Med Res* 1999;**8**:135–160.
- LMSchartmaker Light|Health for all Children.
- Cole TJ. The LMS method for constructing normalized growth standards. *Eur J Clin Nutr* 1990;**44**:45–60.
- WHO. *WHO Child Growth Standards: Methods and Development*. WHO 2014 Available online at: <https://www.who.int/publications/i/item/924154693X>
- Kulaga Z, Grajda A, Gurzowska B, Gózdź M, Wojtyła M, Świąder A, et al. Polish 2012 growth references for preschool children. *Eur J Pediatr* 2013;**172**:753–761.
- Kulaga Z, Litwin M, Tkaczyk M, Rózdzyńska A, Barwicka K, Grajda A, et al. The height-, weight-, and BMI-for-age of Polish school-aged children and adolescents relative to international and local growth references. *BMC Public Health* 2010;**10**:109.
- Albakheet SS, Lee M-J, Yoon H, Shin HJ, Koh H. Psoas muscle area and paraspinal muscle fat in children and young adults with or without obesity and fatty liver. *PLoS ONE* 2021;**16**:e0259948.
- Byun S-E, Kim S, Kim K-H, Ha Y-C. Psoas cross-sectional area as a predictor of mortality and a diagnostic tool for sarcopenia in hip fracture patients. *J Bone Miner Metab* 2019;**37**:871–879.
- Harbaugh CM, Zhang P, Henderson B, Derstine BA, Holcombe SA, Wang SC, et al. Personalized medicine: Enhancing our understanding of pediatric growth with analytic morphomics. *J Pediatr Surg* 2017;**52**:837–842.
- Orsso CE, Mackenzie M, Alberga AS, Sharma AM, Richer L, Rubin DA, et al. The use of magnetic resonance imaging to characterize abnormal body composition phenotypes in youth with Prader-Willi syndrome. *Metabolism* 2017;**69**:67–75.
- Locke JE, Carr JJ, Nair S, Terry JG, Reed RD, Smith GD, et al. Abdominal lean muscle is associated with lower mortality among kidney waitlist candidates. *Clin Transplant* 2017;**31**:e12911.
- Reid JG, Livingston LA, Pearsall DJ. The geometry of the psoas muscle as determined by magnetic resonance imaging. *Arch Phys Med Rehabil* 1994;**75**:703–708.
- Been E, Shefi S, Kalichman L, Bailey JF, Soudack M. Cross-sectional area of lumbar spinal muscles and vertebral endplates: a secondary analysis of 91 computed tomography images of children aged 2-20. *J Anat* 2018;**233**:358–369.
- WHO. *Executive Summary*. WHO 2014 Available online at: <https://www.who.int/childgrowth/standards/velocity/tr3summary.pdf>
- Kalka E, Pastuszak A, Buško K. Secular trends in body height, body weight, BMI and fat percentage in Polish university students in a period of 50 years. *PLoS ONE* 2019;**14**:e0220514.
- Pescatori LC, Savarino E, Mauri G, Silvestri E, Cariati M, Sardaneli F, et al. Quantifica-

- tion of visceral adipose tissue by computed tomography and magnetic resonance imaging: reproducibility and accuracy. *Radiol Bras* 2019;**52**:1–6.
38. Ortega X, Araneda D, Asahi T, Corral G, Rojas G, Suarez B, et al. Variability of muscle fat fraction quantification in MRI using the Dixon technique. *Rev Chil Radiol* 2016;**22**:149–157.
39. Murphy AJ, White M, Elliott SA, Lockwood L, Hallahan A, Davies PS. Body composition of children with cancer during treatment and in survivorship. *Am J Clin Nutr* 2015;**102**:891–896.
40. Rahemi H, Nigam N, Wakeling JM. The effect of intramuscular fat on skeletal muscle mechanics: implications for the elderly and obese. *J R Soc Interface* 2015;**12**:20150365.

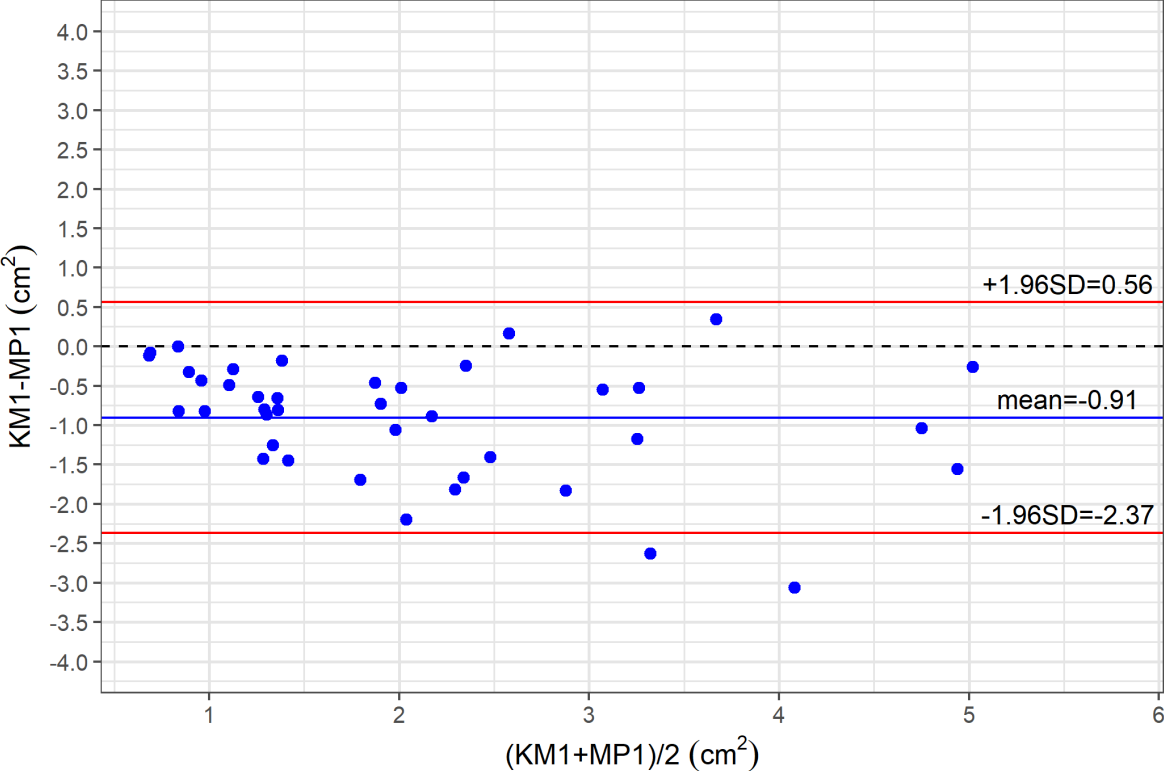
Supplementary figure 1. Bland-Altman plot of the difference in interobserver tPMA segmentation (cm^2) against the mean tPMA segmentation (cm^2). KM, first radiologist; MP, second radiologist; tPMA, total Psoas Muscle Area; SD, standard deviation.



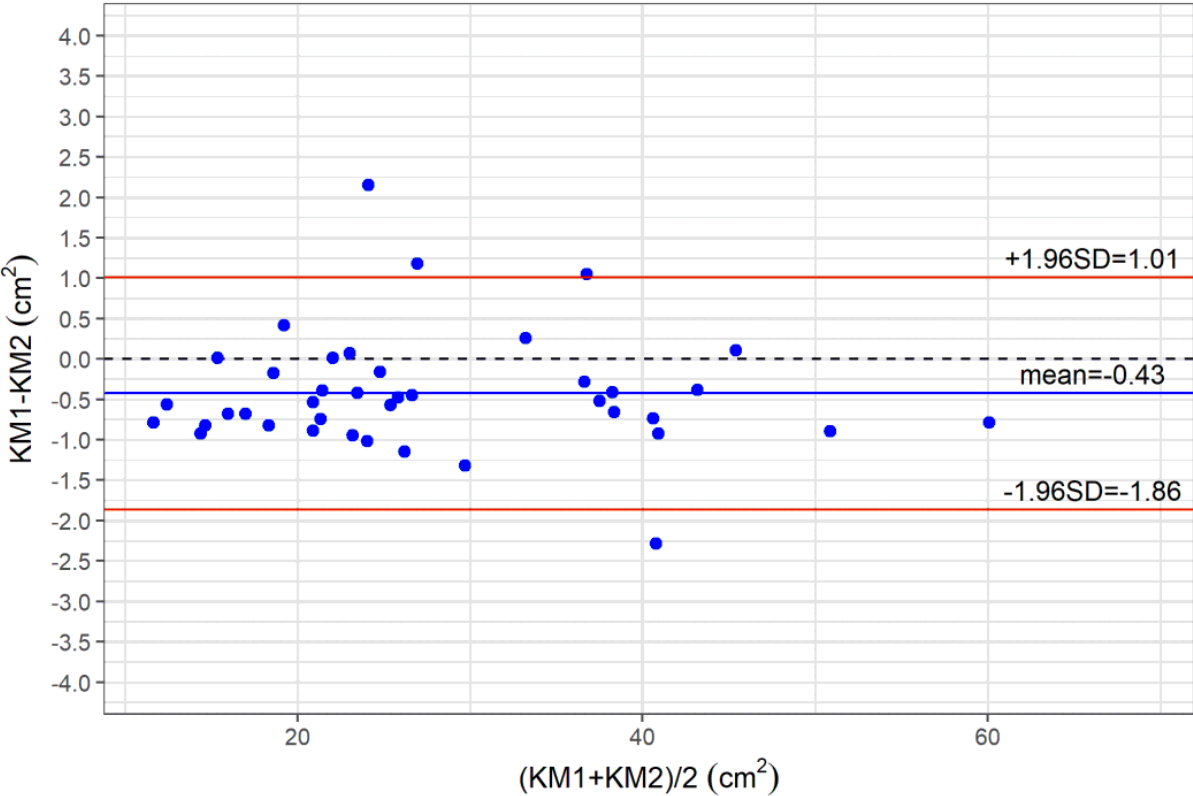
Supplementary figure 2. Bland-Altman plot of the difference in interobserver tPSMA segmentation (cm^2) against the mean tPSMA segmentation (cm^2). KM, first radiologist; MP, second radiologist; tPSMA, total Paraspinal Muscle Area; SD, standard deviation.



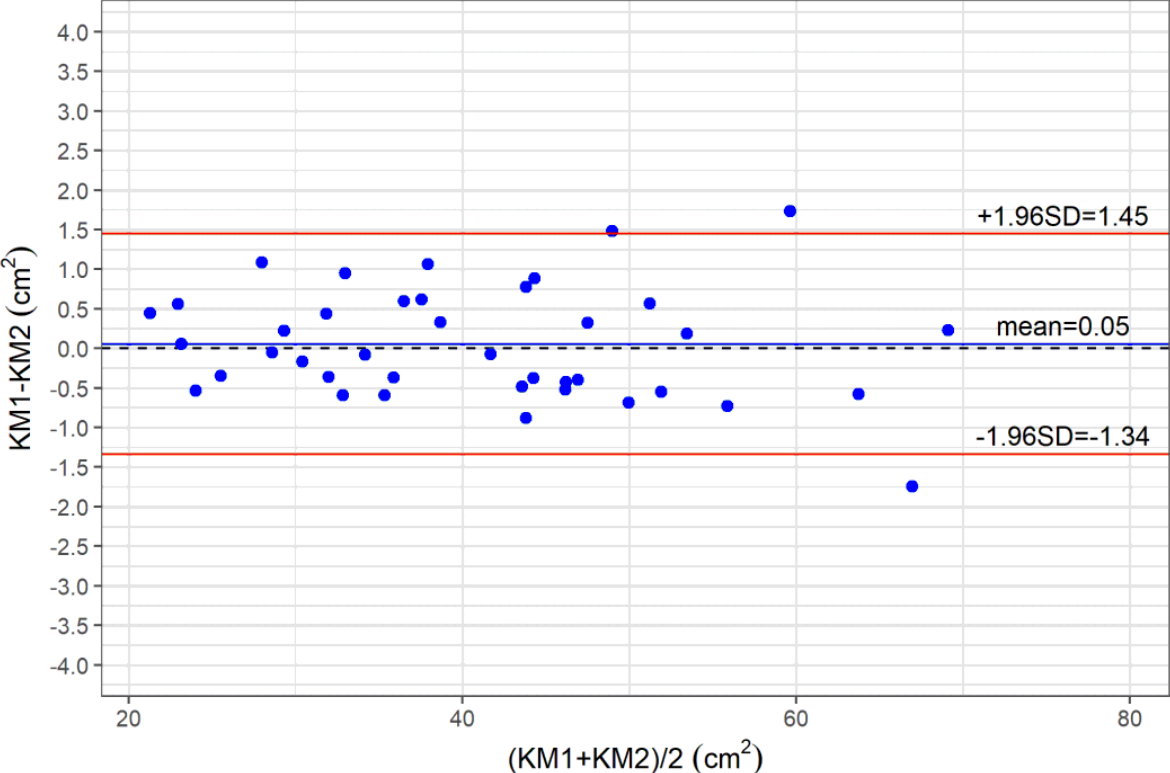
Supplementary figure 3. Bland-Altman plot of the difference in interobserver tMFI segmentation (cm^2) against the mean tMFI segmentation (cm^2). KM, first radiologist; MP, second radiologist; tMFI, total Macroscopic Fat Infiltrations of the paraspinal muscle area; SD, standard deviation.



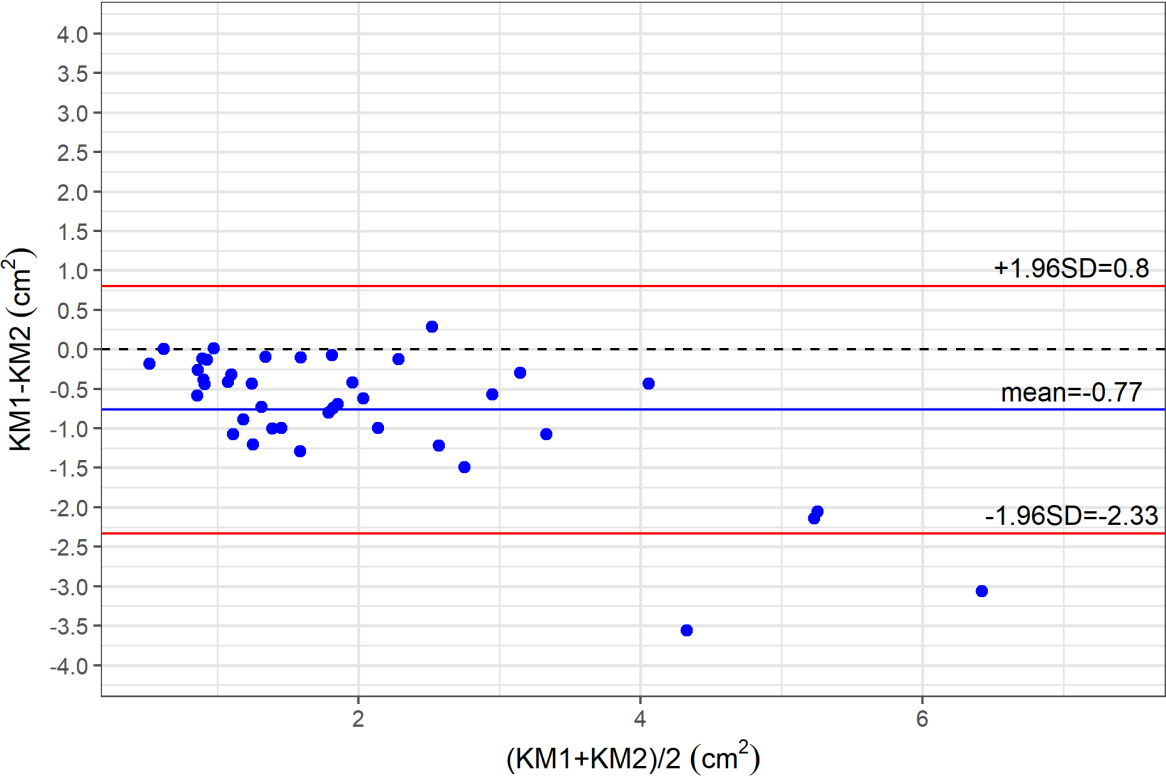
Supplementary figure 4. Bland-Altman plot of the difference in intraobserver tPMA segmentation (cm^2) against the mean tPMA segmentation (cm^2). KM₁, first radiologist, first measurement; KM₂, first radiologist, second measurement; tPMA, total Psoas Muscle Area; SD, standard deviation.



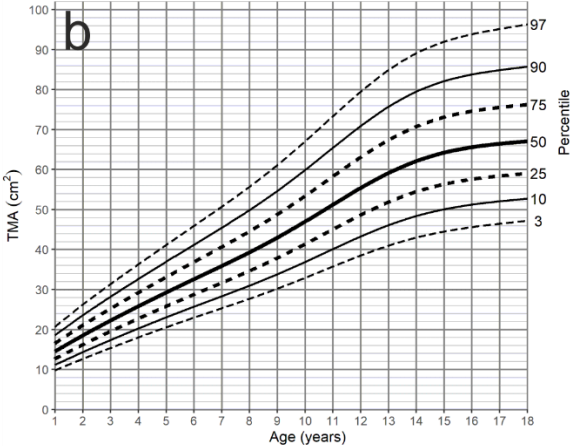
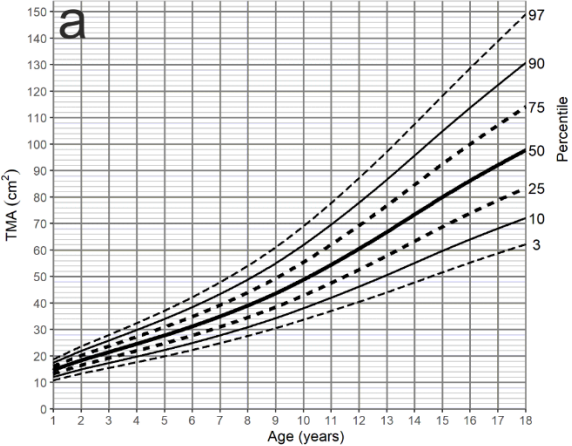
Supplementary figure 5. Bland-Altman plot of the difference in intraobserver tPSMA segmentation (cm^2) against the mean tPSMA segmentation (cm^2). KM_1 , first radiologist, first measurement; KM_2 , first radiologist, second measurement; tPSMA, total Paraspinal Muscle Area; SD, standard deviation.



Supplementary figure 6. Bland-Altman plot of the difference in intraobserver tMFI segmentation (cm^2) against the mean tMFI segmentation (cm^2). KM_1 , first radiologist, first measurement; KM_2 , first radiologist, second measurement; tMFI, total Macroscopic Fat Infiltrations of the paraspinal muscle area; SD, standard deviation.



Supplementary figure 7. Total muscle area-for-age (cm²) percentile charts for **a.** boys and **b.** girls aged from 1 to 18 years. TMA, Total Muscle Area.



Supplementary figure 8. Study cohort differentiated by sex and age.

